BAMS Article

The NCAR GPS Dropwindsonde and Its Impact on Hurricane Operations and Research

Sim D. Aberson, Jun A. Zhang, Jonathan Zawislak, Kathryn Sellwood, Robert Rogers, and Joseph J. Cione

KEYWORDS: Hurricanes/typhoons; Tropical cyclones; Dropsondes; Soundings

ABSTRACT: The global positioning system dropwindsonde has provided thousands of high-resolution kinematic and thermodynamic soundings in and around tropical cyclones (TCs) since 1997. These data have revolutionized the understanding of TC structure, improved forecasts, and validated observations from remote sensing platforms. About 400 peer-reviewed studies on TCs using these data have been published to date. This paper reviews the history of dropwindsonde observations, changes to dropwindsonde technology since it was first used in TCs in 1982, and how the data have improved forecasting and changed our understanding of TCs.

https://doi.org/10.1175/BAMS-D-22-0119.1
Corresponding author: Sim D. Aberson, sim.aberson@noaa.gov
In final form 16 September 2023

AFFILIATIONS: Aberson, Rogers, and Cione—NOAA/OAR/Atlantic Oceanographic and Meteorological Laboratory, Miami, Florida; **Zhang and Sellwood**—NOAA/OAR/Atlantic Oceanographic and Meteorological Laboratory, and Cooperative Institute for Marine and Atmospheric Studies, University of Miami, Miami, Florida; **Zawislak**—NOAA/OAR/Atlantic Oceanographic and Meteorological Laboratory, and Cooperative Institute for Marine and Atmospheric Studies, University of Miami, Miami, and NOAA/OMAO/Aircraft Operations Center, Lakeland, Florida

The global positioning system (GPS) dropwindsonde (Hock and Franklin 1999) takes high-resolution pressure, temperature, humidity, and wind velocity measurements as it descends from aircraft. It is the culmination of improvements to instruments, tracking techniques, and data transmission that resulted in the balloon-launched radiosonde (or rawinsonde) used today (Fig. 1). This technology had historically been used to obtain vertical soundings upward from the Earth's surface; in 1949, the U.S. military noted that they could measure surface pressure by releasing a radiosonde without the balloon from aircraft. The instrument was dubbed the dropsonde as the wind-finding capability had not yet been developed. Aircraft crews soon started regular dropsonde releases into tropical cyclone (TC) eyes to measure surface pressure; the first such release in the Atlantic was in Hurricane Able in 1950 (Hagen et al. 2012). A history of the development of the dropsonde is available in Dabberdt et al. (2022).

The National Center for Atmospheric Research (NCAR) led the development of a dropwindsonde (renamed due to its ability to measure wind velocity) using the Omega navigation system that became available in 1971 (Govind 1975; Simpson et al. 1975). This Omega dropwindsonde (ODW) was used during the Global Atlantic Research Program (GARP) Atlantic Tropical Experiment (GATE). The real-time data were coarse, mainly at mandatory pressure levels below the aircraft with the later addition of significant levels, and the wind finding (the process by which winds are calculated from the instrument motion) did not consistently work in clouds, prohibiting observations in TC eyewalls, nor during aircraft maneuvers (Franklin and Julian 1985). Postflight data were available at 10-s intervals for thermodynamic data and at 30-s intervals for wind. The ODW did provide the first reliable and frequent soundings in the oceanic TC environment. Joanne Simpson sought other uses of the instrument after GATE. Bob Burpee noted that an important reason for TC forecast failures was the lack of observations in the TC environment. They came up with the idea to drop ODWs from the aircraft for assimilation into operational numerical models, and the ODW was adopted for use by both NOAA and the U.S. Air Force. On 15 September 1982, the first "synoptic flow" mission was conducted around Hurricane Debby (Burpee et al. 1984). Even though only 17 such missions were flown by 1996, improved modeling and data assimilation techniques allowed scientists to show that the ODW data allowed for a 16%–30% reduction in track forecast errors in the cases flown, improvements that were as large as the cumulative error reduction during the previous 20–25 years (Franklin and DeMaria 1992; Burpee et al. 1996). Partly as a result, Congress authorized NOAA to purchase a Gulfstream-IV (G-IV) high-altitude jet to fly operational missions when TCs threatened the United States (Aberson and Franklin 1999). The new GPS technology replaced Omega, and by late 1996, the new GPS dropwindsonde and the Airborne Vertical Atmospheric Profiling System (AVAPS),

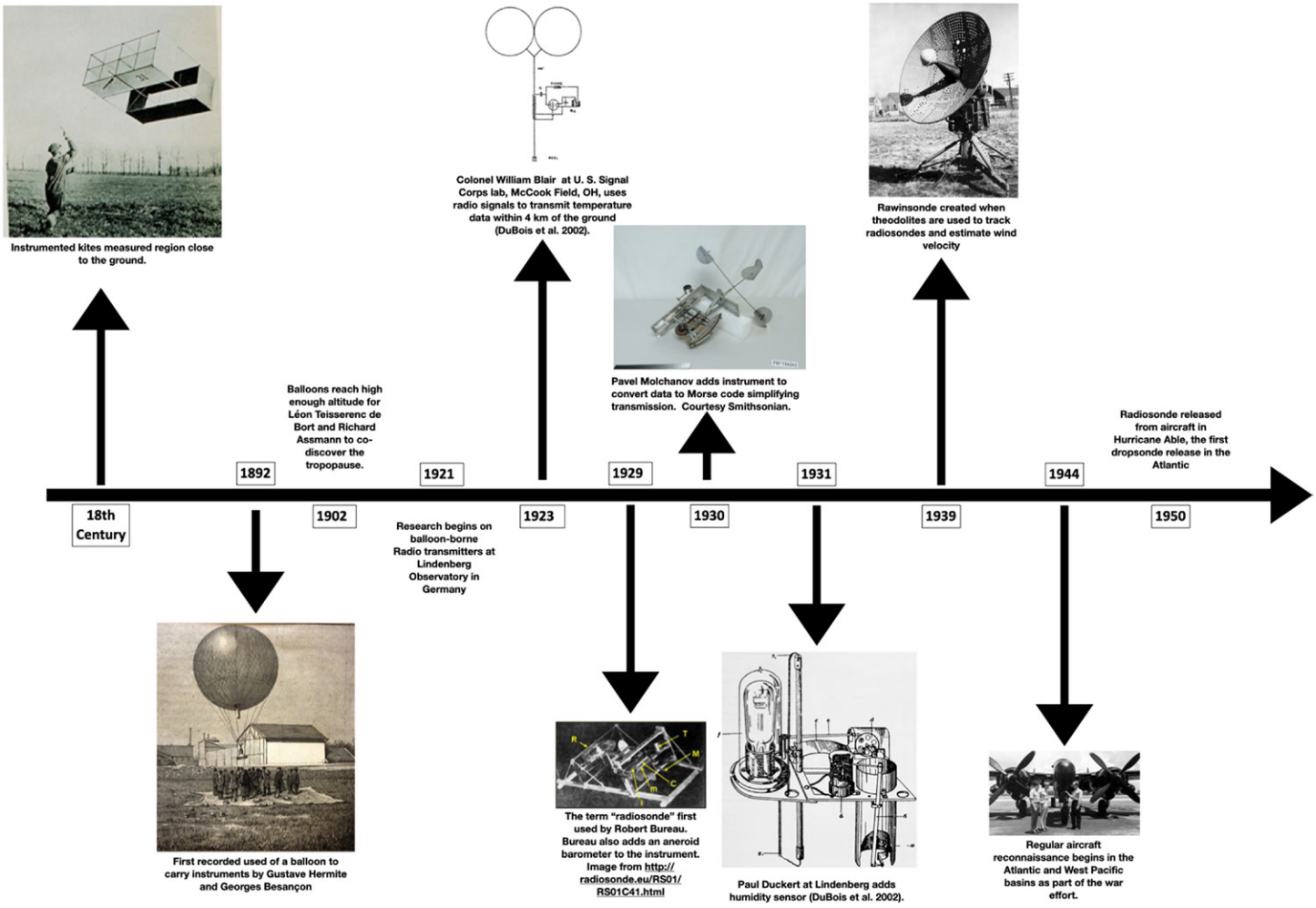

Fig. 1. Timeline of the development of atmospheric sounding technology through the advent of dropwindsondes.

also developed by NCAR, replaced the ODW (Hock and Franklin 1999).[1] The first operational surveillance mission with the new dropwindsonde system was conducted in July 1997 around Tropical Storm Claudette, but the G-IV flew only three missions in the Atlantic that year due to the very inactive season (Aberson and Franklin 1999; Aberson 2002).

[1] An instrument based on the Long Range Navigation (LORAN) system was also developed, but not used in TC research or operations.

On 3 August 1997, during a P-3 research mission in Hurricane Guillermo, Michael Black decided to deploy a GPS dropwindsonde in an eyewall for the first time. The first-ever high-resolution wind and thermodynamic data were obtained in the eyewall, including a wind speed of >78 m s^{-1} (Lawrence 1999). Since then, the dropwindsonde system has been installed on additional aircraft around the world, including a modified system for the NASA Global Hawk (Wick et al. 2018). Tens of thousands of dropwindsondes have been released in and around TCs worldwide (Fig. 2), revolutionizing TC science, and about 400 research papers have been published in peer-reviewed journals. A continuously updated dropwindsonde data archive in and around TCs is maintained by the Atlantic Oceanographic and Meteorological Laboratory (AOML) Hurricane Research Division (HRD). The data are organized by year, storm name, and aircraft mission and are available at https://www.aoml.noaa.gov/data-products/#hurricanedata, with information on the data formats at https://www.aoml.noaa.gov/hrd/Storm_pages/sondeformat.html. This paper reviews major changes to GPS dropwindsonde use and technology since 1997, and how the data have improved forecasts and changed understanding of TCs.

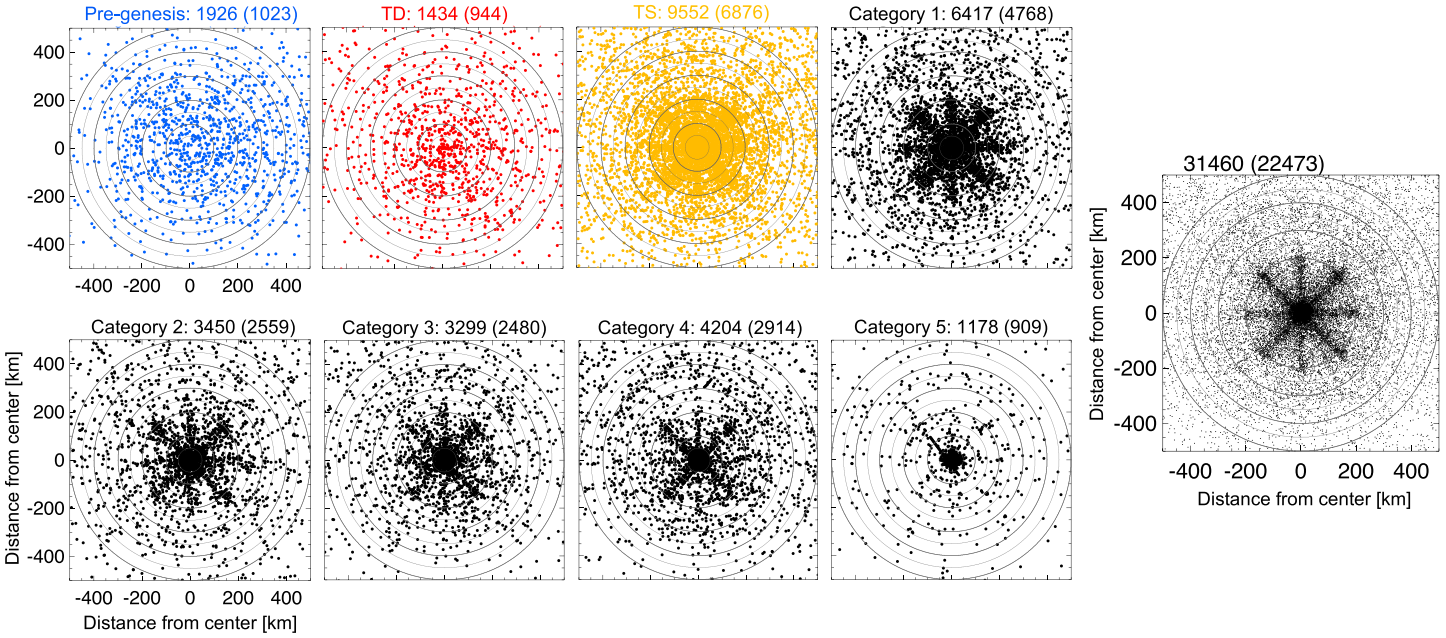

Fig. 2. Storm-relative locations of dropwindsonde releases in various TC stages from 1996 through 2021. (right) A composite of all the dropwindsonde releases. The total number in each life cycle stage is indicated above each panel, with the total number within 500 km of the TC center in parentheses.

History of the GPS dropwindsonde and quality control procedures

The first GPS dropwindsonde (Hock and Franklin 1999), the RD93, was produced from 1996 to 2009. This version used a "codeless" GPS receiver (Kaisti 1995) to calculate the wind velocity. The GPS receiver tracked the relative Doppler frequencies from satellite signals, so no positions or velocities were calculated on the instrument itself. The relative Doppler frequencies corresponded to the combined motions of the satellites and the receiver, and the GPS processing card in the aircraft data system converted them to wind velocity. Starting with the RD94 dropwindsonde, a GPS receiver that calculates the location of the instrument itself has been used, thus allowing for more accurate and reliable wind velocity measurements than before, especially in high wind speed regions near the surface. That version also allowed for an increased data rate for the wind velocity. The subsequent upgrade to the RD41 system in 2018 provided additional improvements. Miniaturized versions of the last two (NRD94 and NRD41) have also been manufactured, and the NRD41 dropwindsonde is due to become the main instrument in TC operations in 2023. Some instruments were outfitted with an infrared (IR) sensor (Fig. 3) to provide sea surface[2] temperature measurements along with the other observations. Specifications of these instruments are provided in Table 1.

[2] The instrument may also provide the temperature of cloud tops if it is released in clear air, though this has not been tested extensively.

The original processing and quality-control software, known as "editsonde," was written and maintained by AOML/HRD and installed on the NOAA aircraft to facilitate real-time data transmission so that the data could be used by forecasters and be assimilated into numerical models. Editsonde was also used postflight to create research-quality datasets. Because the graphical interface was designed to use Hewlett-Packard libraries (Griffin et al. 1992), editsonde could not be converted easily to other computer systems. NCAR developed the Atmospheric Sounding Processing Environment (ASPEN), based on editsonde algorithms, which is now used on all aircraft and for postflight research. Editsonde required frequent manual intervention during quality control; ASPEN was designed to operate as automatically as possible using a graphical user interface, while allowing for manual intervention when required.

Both software packages identify the sounding termination (usually splash) point and apply an automated algorithm sequence to flag erroneous data. Corrections for the wind shear and thermal-sensor lags are applied, and a filter eliminates aliasing of unresolvable scales (i.e., scales of ~3 s or less) (Hock and Franklin 1999). The final products are the quality-controlled data in multiple formats including TEMP DROP, Binary Universal Form for the Representation of meteorological data (BUFR), full-resolution data (FRD) files, and Network Common Data Form (NetCDF) files. Skew T–log$p$ diagrams of individual soundings and synoptic station plots can be produced, and other files contain information on the quality-control procedures that were used.

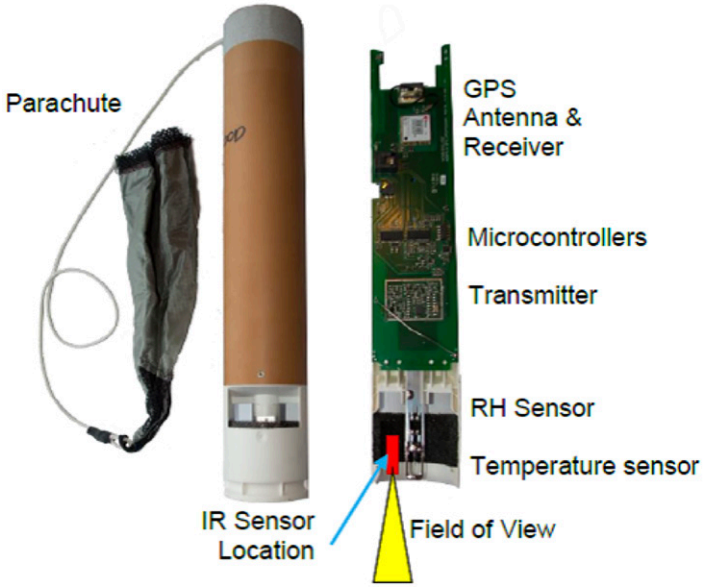

Fig. 3. (left) View of a standard dropwindsonde and (right) inside view of all sensors showing location of additional IR sensor. From Zhang et al. (2017).

Table 1. Specifications of the various GPS dropwindsonde systems in use. Repeatability refers to the standard deviation of differences between two successive repeated calibrations. (Information courtesy of Vaisala, Inc., manufacturer of the RD instruments, and NCAR, producer of the NRD instruments.)

	RD93	RD94	NRD94	RD41	NRD41
Year introduced	1996	2009	2010	2018	2018
Diameter (cm)	7.0	7.0	4.5	7.0	4.5
Length (cm)	41.0	41.0	30.5	41.0	30.5
Weight (g)	400	350	167	350	169
Parachute size (cm)	30 × 30	30 × 30	20 × 20	30 × 30	20 × 20
Pressure (hPa)	Range: 3–1,080 Repeatability: 0.4 Resolution: 0.1 Data rate: 2 Hz	Range: 3–1,080 Repeatability: 0.4 Resolution: 0.01 Data rate: 2 Hz		Range: 3–1,080 Repeatability: 0.4 Resolution 0.01 Data rate: 2 Hz	
Temperature (°C)	Range: −90 to 60 Repeatability: 0.2 Resolution: 0.1 Data rate: 2 Hz	Range: −90 to 60 Repeatability: 0.2 Resolution: 0.1 Data rate: 2 Hz		Range: −90 to 60 Repeatability: 0.1 Resolution: 0.01 Data rate: 2 Hz	
Humidity (%)	Range: 0–100 Repeatability: 2 Resolution: 1 Data rate: 2 Hz	Range: 0–100 Repeatability: 2 Resolution: 1 Data rate: 2 Hz		Range: 0–100 Repeatability: 2 Resolution: 0.1 Data rate: 2 Hz	
Horizontal wind (m s^{-1})	Range: 0–200 Accuracy: ±0.5 Resolution: 0.1 Data rate: 2 Hz Codeless GPS	Range: 0–200 Accuracy: ±0.5 Resolution: 0.1 Data rate: 4 Hz Code-correlating GPS		Range: 0–200 Accuracy: ±0.5 Resolution: 0.1 Data rate: 4 Hz Code-correlating GPS	

Real-time and best-track intensity estimation

Before the advent of the GPS dropwindsonde, the main technique to estimate TC intensity (defined as the maximum sustained, or time-averaged, wind speed at 10-m altitude) from aircraft measurements was to adjust aircraft flight-level wind speed measurements downward by 10%–20% (Franklin et al. 2003). The first operational use of dropwindsonde data in the TC eyewall occurred in Hurricane Georges (1998) when it was near peak intensity. NHC's Tropical Cyclone Discussions made numerous references to eyewall dropsonde wind reports, and in postanalysis, Georges' assigned intensity of 135 kt (1 kt ≈ 0.51 m s^{-1}) was based largely on these data. The measured low-level wind speed was comparable to that at the 3-km flight level, but subsequent observations in Georges during its weakening phase reported low-level wind speed 20%–30% below that at flight level (Pasch et al. 2001). Franklin et al. (2003) quantified adjustments between maximum flight-level and surface wind speeds based on dropwindsonde data and noted that they varied with azimuth and distance from the TC center. Noting that the dropwindsonde measures effectively instantaneous wind velocity, whereas operational centers quantify intensity based on a sustained (time-averaged) wind speed, they calculated a relationship between the mean wind speed in the lowest 150 m of the sounding (corresponding to measurements averaged for about 15 s), the height of the midpoint of that layer, and the wind speed at the surface; Fig. 4 shows the current relationship used at the National Hurricane Center for poststorm analysis, and is a close approximation to what is used in operations. The mean wind speed calculated in the lowest 150 m of the profile was subsequently included in the TEMP-DROP message, and these data have been instrumental in real-time analysis of TC intensity. Even with the advent of the Stepped-Frequency Microwave Radiometer (SFMR; Uhlhorn and Black 2003), such wind speed reductions remain important for TC intensity diagnosis.

The varying and uncertain reduction factor from flight level to the surface is a major factor in the Atlantic hurricane reanalysis project, a reevaluation of past TC tracks and intensities like that of Hurricane Andrew (Dunion et al. 2003; Landsea et al. 2004, 2008, 2012, 2014; Kieper et al. 2016; Hagen et al. 2012; Delgado et al. 2018). Further research into reductions of flight-level wind measurements to the surface (e.g., Powell et al. 2009; Uhlhorn et al. 2014) and refinements to surface wind speed retrievals from SFMR are ongoing.

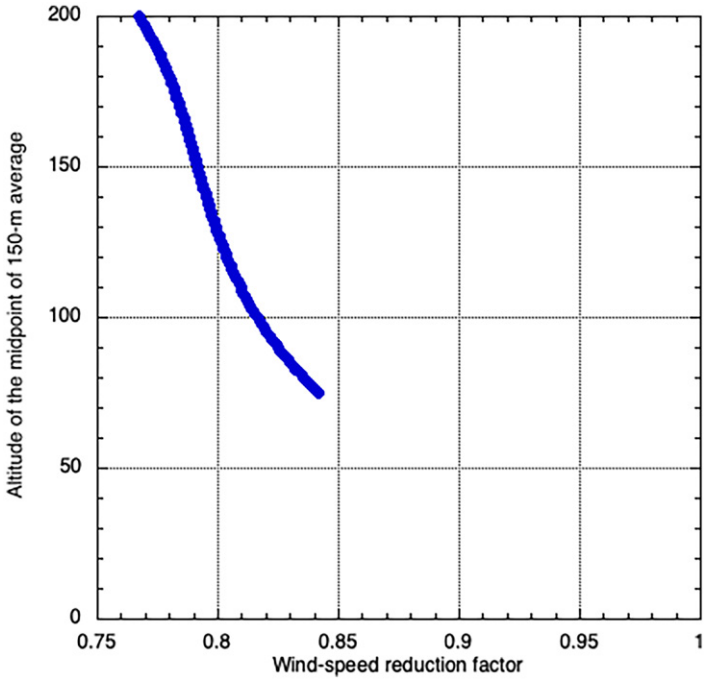

Fig. 4. Reduction factor between the mean wind speed in the lowest 150 m of a dropwindsonde sounding and the surface wind speed in relation to the height of the midpoint of the 150-m layer. This height varies due to failures of the instrument before reaching the surface. This factor is used operationally at the National and Central Pacific Hurricane Centers.

Observing system validation

Because they are in situ measurements with known error characteristics, dropwindsonde data are used for comparison with, and calibration of, other observing systems critical for real-time and postseason TC intensity and structure analyses and for assimilation into numerical forecast. They have validated atmospheric

motion vectors (Dunion and Velden 2002; Dunion et al. 2002; Sears and Velden 2012), surface wind speed measurements from the SFMR (Uhlhorn and Black 2003; Uhlhorn et al. 2007; Powell et al. 2009; Klotz and Uhlhorn 2014; Holbach et al. 2018; Sapp et al. 2019), *Aqua* Moderate Resolution Imaging Spectroradiometer profiles (Zhang et al. 2006), Doppler wind lidar measurements (Bucci et al. 2018; Zhang et al. 2018), Special Sensor Microwave Imager and Quick Scatterometer surface wind speed observations (Chen 2007; Chou et al. 2010), and Synthetic Aperture Radar retrieved wind directions (Gao et al. 2018). They validate high wind speed model functions for scatterometers (Brown and Zeng 2002) and other dropwindsonde systems such as the High-Definition Sounding System (Black et al. 2017). Cione et al. (2016, 2020) used dropwindsondes to corroborate observations from small uncrewed aircraft deployed in Hurricanes Edouard (2014), Maria (2017), and Michael (2018). Dropwindsonde data composites confirmed other near-surface boundary layer thermodynamic measurements (Wadler et al. 2022).

Forecast impact, data assimilation, and targeted observations

NOAA models with data assimilation systems incorporated the dropwindsonde temperature and wind information as soon as the data became available in 1997; moisture data were not used due to potential observational error and deficiencies in the assimilation systems. During the first few years of operational synoptic surveillance with the G-IV, only modest improvements to model forecasts of TC track and intensity were seen. The issue was not the dropwindsonde data themselves, but in how they were assimilated into the models with the then-current three-dimensional variational scheme (Aberson 2002). Aberson (2008) noted forecast degradations due to the assimilation of erroneous data and data in the TC eyewall (that the models at the time could not represent due to their low resolutions) into the models. Operational data processing, quality control, and data assimilation systems have been improved to address these problems (Aberson 2010).

Observing strategies to optimize and maximize the impact of dropwindsonde observations on numerical model forecasts have been developed. In Aberson (2003), the fastest growing modes, or targets, were identified by areas of large forecast spread in the NCEP ensemble forecasting system; the observing strategy required regularly spaced sampling of the entire target due to the 3D-VAR scheme with isotropic covariances. This targeting technique provided larger improvements with the assimilation of the targeted data subset than when the entire dropwindsonde datasets were assimilated, highlighting a weakness of that data assimilation scheme. That technique, along with a companion scheme utilizing a solution to the traveling-salesman problem (Press et al. 2007), was implemented into operations during the 2008 Atlantic hurricane season, allowing for optimal coverage of the target. Other targeting techniques (Aberson 2010; Reynolds et al. 2013; Majumdar et al. 2013; Wu et al. 2014; Torn 2014) have been developed. Most recently, Ditchek and Sippel (2023) in an observing system experiment found that dropwindsonde data within the TC vortex were most important to intensity and structure forecasts and that dropwindsonde data should be obtained close to the center (i.e., the eye and eyewall) of intense TCs for optimal improvement. They also found that not sampling a TC at all is better than only sampling the inner core, confirming the 2018 decision to regularly release dropwindsondes at the end of each radial leg. Further improvements to the operational targeting technique (e.g., Ancell and Hakim 2007; Torn and Hakim 2008) are being tested for operational implementation.

Additional forecast improvements coincided with improved assimilation techniques and assimilation of additional data and the ability to obtain observations from altitudes near and above the tropopause. The first use of dropwindsonde humidity data in global models led to forecast track improvements as large as those from assimilating the wind data (Kamineni et al. 2006); NCEP began assimilating dropwindsonde humidity measurements

into their operational models a few years later. Since dropwindsondes are advected by the wind, they have been seen to drift more than halfway around the eyewall in intense TCs; only the launch location is available in the original TEMP DROP message, so a technique to calculate the location of each observation in the message (Aberson et al. 2017a) allows for the assimilation of dropwindsonde data in high-resolution model systems. Christophersen et al. (2017, 2018a,b) and Kren et al. (2018) assessed the impact of dropwindsonde data in the stratosphere and upper troposphere during the Hurricane and Severe Storm Sentinel (Braun et al. 2016) and Sensing Hazards with Operational Unmanned Technology (Wick et al. 2018) programs, confirming the additive impact of dropwindsonde data when mixed with other data types like those now available from low-orbit satellites. The first attempt to assimilate dropwindsonde data using an ensemble Kalman filter (Aberson and Etherton 2006) was soon followed by significant improvements to that methodology (Torn and Hakim 2008) and implementation of ensemble-based data assimilation systems in numerical model systems globally.

The success of targeted dropwindsonde observations in the Atlantic and eastern North Pacific basins led Taiwan to institute their own aircraft-based program, the Dropwindsonde Observations for Typhoon Surveillance near the Taiwan Region (DOTSTAR). Other programs in the western North Pacific basin followed (Wu et al. 2007a,b; Chou and Wu 2008; Yamaguchi et al. 2009; Reynolds et al. 2010; Chou et al. 2011; Xie et al. 2013; Holt et al. 2015).

Characterizing and understanding physical structures and processes

Dropwindsonde data have greatly improved understanding of TC dynamics and thermodynamics, leading to improvements to models and parameterization schemes and official forecasts of track, intensity, and structure. Some understandings may not translate directly to changes to operational models or products, but may be incorporated indirectly into manual forecast techniques used by specialists to make forecasts, especially of intensity and structure. The data have been used directly to validate and improve models that are the bases for official forecasts.

High-resolution observations in the TC boundary layer were very rare until the late 1990s. Wind speed within the boundary layer was thought to decrease from gradient flow at the top with a progressive turning of the wind toward the TC center near the surface, though some previous observations suggested the presence of a supergradient low-level jet (Kepert 2001). Dropwindsonde data show substantial variability in boundary layer structure, especially in the inflow angle (Zhang and Uhlhorn 2012), and that a low-level wind speed maximum is common (Kepert 2001; Kepert and Wang 2002; Giammanco et al. 2013). The heights of this jet and of the boundary layer top were found to decrease with decreasing radius from the TC center, and the jet is strongest on the motion-relative left side of the TC (Kepert 2006a,b; Schwendike and Kepert 2008; Zhang et al. 2011). Improved boundary layer models were developed as a result (Vickery et al. 2009; Lee and Chen 2012; Snaiki and Wu 2018) and underscored the threat to high-rise structures noted by Franklin et al. (2003). Emergency managers had once suggested "vertical evacuation" to keep people safe from storm surge, but these new findings changed these recommendations to make such evacuation a last resort.

Knowledge of the mechanisms by which heat, moisture, and momentum are transferred between the atmosphere and the ocean is necessary to improve numerical model forecasts, especially of TC intensity. Since high-resolution near-surface wind measurements were difficult to obtain in high-wind regimes, values of parameters such as surface stress, roughness length, and drag coefficients were extrapolated from measurements in low wind speed regimes. Parameters such as momentum and enthalpy fluxes, roughness lengths, and exchange coefficients were estimated for the first time in intense TCs using

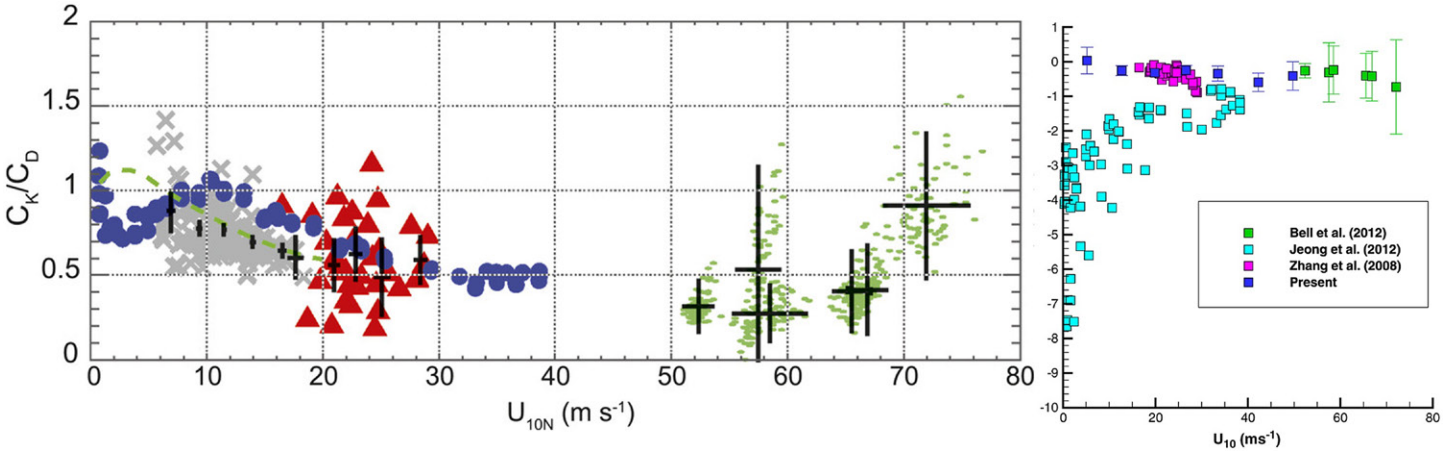

Fig. 5. (left) Neutral drag coefficient (C_{d10N}) as a function of 10-m wind speed (U_{10}). The green circles show results from Bell et al. (2012). Black and blue symbols indicate data adapted from French et al. (2007) and Vickery et al. (2009), respectively. The crosses show mean and standard deviation of C_{d10N} at a given wind speed. (right) Exchange coefficient for enthalpy transfer as a function of U_{10} from multiple studies. The left and right panels were taken from Bell et al. (2012) and Richter and Stern (2014), respectively.

dropwindsonde data (Fig. 5) through profile (Powell et al. 2003; Holthuijsen et al. 2012; Richter and Stern 2014; Richter et al. 2016, 2021) and budget (Bell et al. 2012) methods; vertical eddy diffusivity in the boundary layer was derived with flight-level data using a flux calculation method and dropwindsonde data for a vertical gradient calculation method (Zhang et al. 2011; Zhang and Drennan 2012). The various parameters change with wind velocity, TC region, and sea state. Zhang et al. (2015) presented a feedback framework by which aircraft observations in TCs are used to identify model deficiencies, and new schemes are developed based on these data, with subsequent improvements to model systems, especially in the boundary layer. This developmental framework was successful in improving physics related to turbulent transfer processes, surface layer, boundary layer, and horizontal diffusion parameterization schemes in the operational Hurricane Weather Research and Forecast (HWRF) model, resulting in improved track and intensity forecasts (Zhang et al. 2015). Zhang et al. (2015, 2017) studied the impact of boundary layer physics improvement on HWRF forecasts of two TCs undergoing rapid intensification (RI) and found that observation-based modification of the vertical eddy diffusivity (K_m) in the planetary boundary layer (PBL) scheme (Fig. 6) substantially improved the RI forecasts. The data have been used for model evaluation, especially for new model systems. Liu et al. (2012) used the data to verify forecast models beyond the regular parameters used in TC model evaluation. Bryan et al. (2017), Stern and Bryan (2018), and Stern et al. (2021) used dropwindsonde data to evaluate large-eddy TC simulations, especially in the boundary layer. Details of how the observations led to improvements to operational TC models are presented in Zhang et al. (2020).

Dropwindsonde data helped to define different boundary layers (defined by thermodynamics, kinematics, or multiple parameters) in the TC and allowed for the first detailed look at the thermodynamics and energetics in the TC inflow layer. Traditional methods to define the boundary layer based on the Richardson number are not appropriate to TCs (Fig. 7; Zhang et al. 2011). The height of the top of the boundary layer varies by quadrant (Zhang et al. 2009, 2011, 2013; Ming et al. 2015). Dropwindsonde data illuminated changes to the thermodynamics and energetics along inflow trajectories within the boundary layer (Wroe and Barnes 2003; Schneider and Barnes 2005; Barnes 2008; Barnes and Dolling 2013; Fig. 8) supporting hypotheses that hurricane intensity appears to be strongly modulated

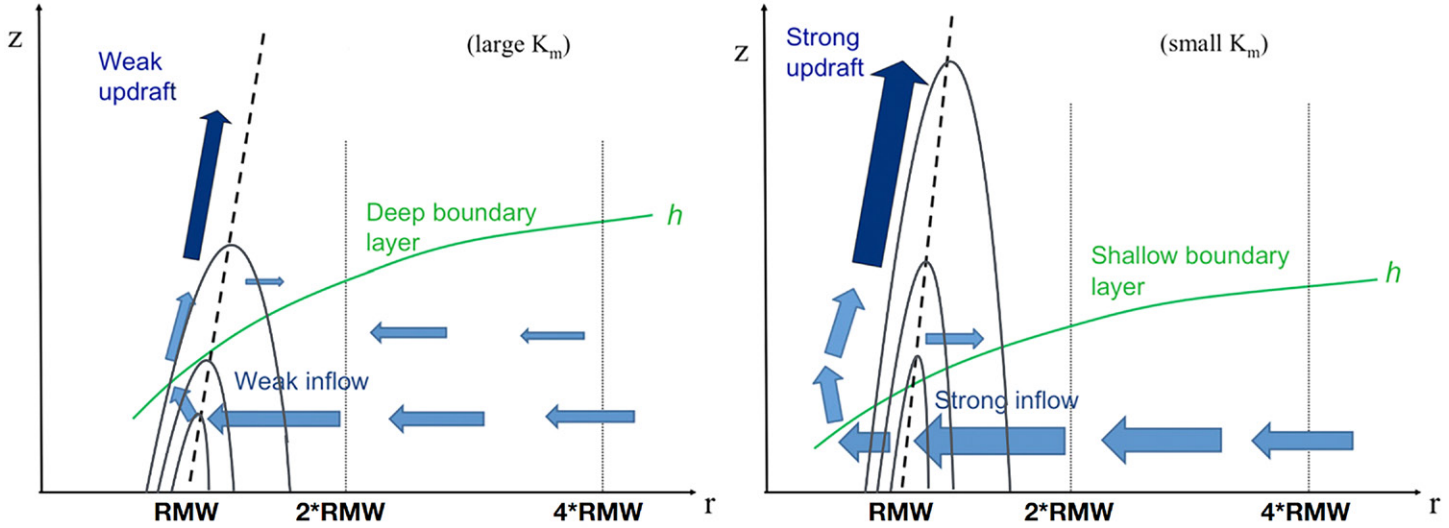

Fig. 6. Height–distance (normalized by the radius of maximum wind speed) schematics showing different structures in Hurricane Weather Research and Forecast Model forecasts with (left) large vertical eddy diffusivity (K_m) and (right) small K_m. The green line denotes the boundary layer height (h). The black dashed line shows the radius of maximum wind speed varying with height (z). The black solid lines are contours of the tangential wind speed, showing the vortex depth. This figure is a modified version of Fig. 17 in Zhang et al. (2015).

by energy exchange near and under the eyewall. Equivalent potential temperature was discovered to be unmixed in the boundary layer several hundred km from the TC center; this was contrary to then-current theory but supported similar findings in numerical simulations (Montgomery et al. 2014). Outside the core, cool and dry convective downdrafts reduce enthalpy in the boundary layer as it is gained from the warm sea below. Surface fluxes increase close to the eyewall, but little energy loss through the layer top is seen. It appears that the TC secondary circulation enhances convection in this region, thus allowing for an increase in energy and supporting the hypothesis that TC intensity is controlled by energy exchanges close to and under the eyewall. The radial wind decelerates

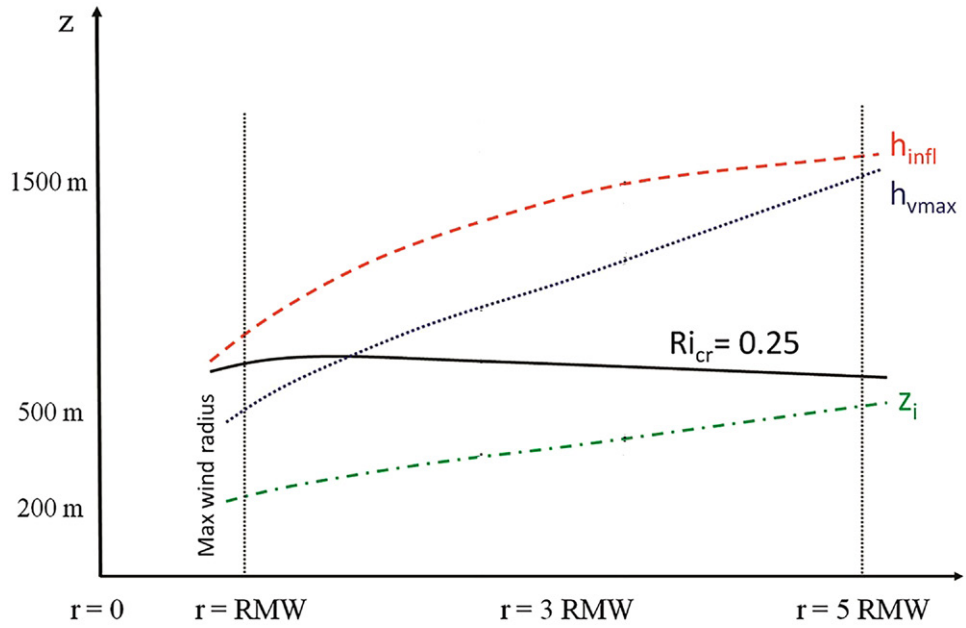

Fig. 7. Schematic of boundary layer height with distance from the center normalized by the radius of maximum wind speed (RMW) based on dropwindsonde composites. Here, h_{infl} is the depth of the inflow layer, z_i is the depth of the mixed layer, and h_{vmax} is the height of the maximum wind speed. The solid black line denotes the height where the bulk Richardson number is equal to 0.25. From Zhang et al. (2011).

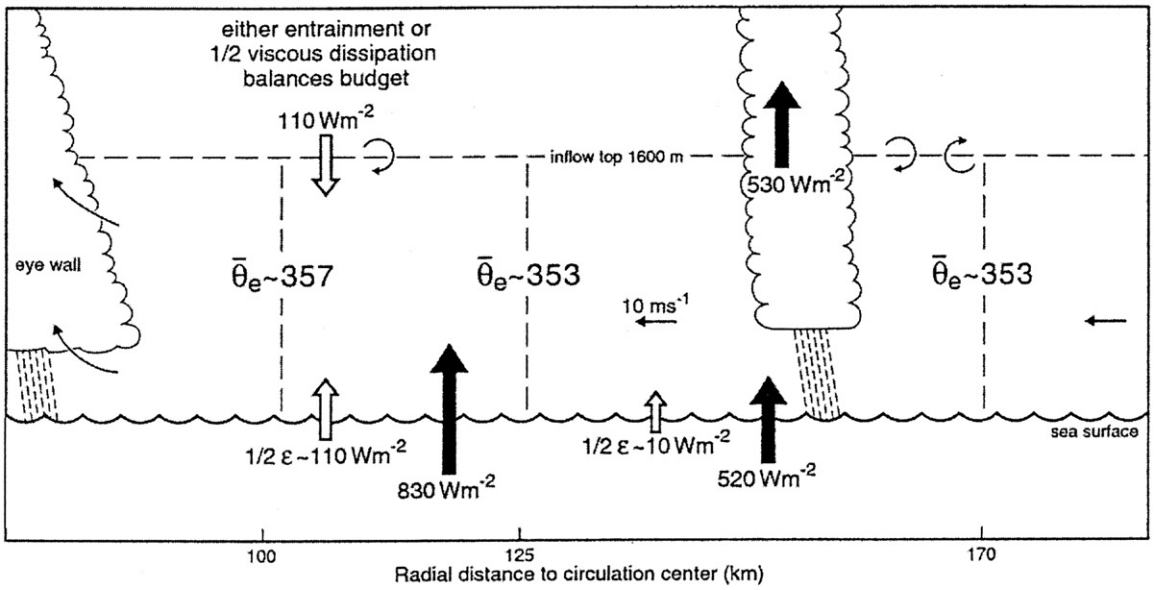

Fig. 8. Schematic of an equivalent potential temperature (θ_e) budget along the inflow trajectory in the boundary layer of Hurricane Bonnie (1998). This figure is from Wroe and Barnes (2003) and is based on dropwindsonde data.

in the boundary layer leading to low-level convergence just inward of the eyewall. This leads to deep convection in the eyewall and is similar whether it occurs in the primary or secondary eyewall during a replacement cycle (Bell et al. 2012; Abarca et al. 2016). These studies and others (Montgomery et al. 2014; Rogers et al. 2015, 2016; Zawislak et al. 2016) found gradient imbalances in dropwindsonde data during intensification.

TCs in low-shear environments tend to intensify, and those in highly sheared environments tend to weaken. In moderately shear environments (9–22 kt; Rios-Berrios and Torn 2017), TCs do everything from rapidly intensify to weaken, increasing the difficulty of some forecasts. Rogers et al. (2015, 2016), Zawislak et al. (2016), and Nguyen et al. (2017) found that shear-related asymmetries in precipitation, humidity, entropy, and temperature contribute to TC intensity changes (Fig. 9). Dropwindsonde data showed that dry layers originate from dynamically forced and precipitation-driven subsidence in the upshear hemisphere; these layers hinder intensification as they increase stability, cap the boundary layer, and suppress convection. Nguyen et al. (2017), Wadler et al. (2018), and Rogers et al. (2020) found that convective downdrafts in the left-of-shear and upshear quadrants sometimes carry low-entropy air downward, cooling and stabilizing the low levels downstream. This stabilization can inhibit the development of precipitation symmetrically around the storm, limiting intensification. However, the air recovers entropy through surface enthalpy fluxes as it circulates toward the downshear-right quadrant, favoring intensification (Zhang et al. 2017; Nguyen et al. 2019; Wadler et al. 2022), and midtropospheric moistening from convection may remove dry layers aloft (Zawislak et al. 2016). Nguyen et al. (2019) found, by compositing a large number of dropwindsonde observations in and around weak TCs, that conditional instability is maximized downshear and minimized upshear regardless of intensity change, but that stability decreases with intensification rate due to increased moist entropy in the boundary layer.

Dropwindsondes have observed mesoscale and misoscale features in eyes and eyewalls of intense TCs, though it remains unclear whether these features have any impact on TC intensity or structure. These features may increase TC intensity and produce vertical motions that create hazards for reconnaissance aircraft and may be responsible for catastrophic damage over land (Montgomery et al. 2006; Aberson et al. 2006; Bell and Montgomery 2008; Sanger et al. 2014; Nugent and Rios-Berrios 2018). Stern et al. (2016) found that these features,

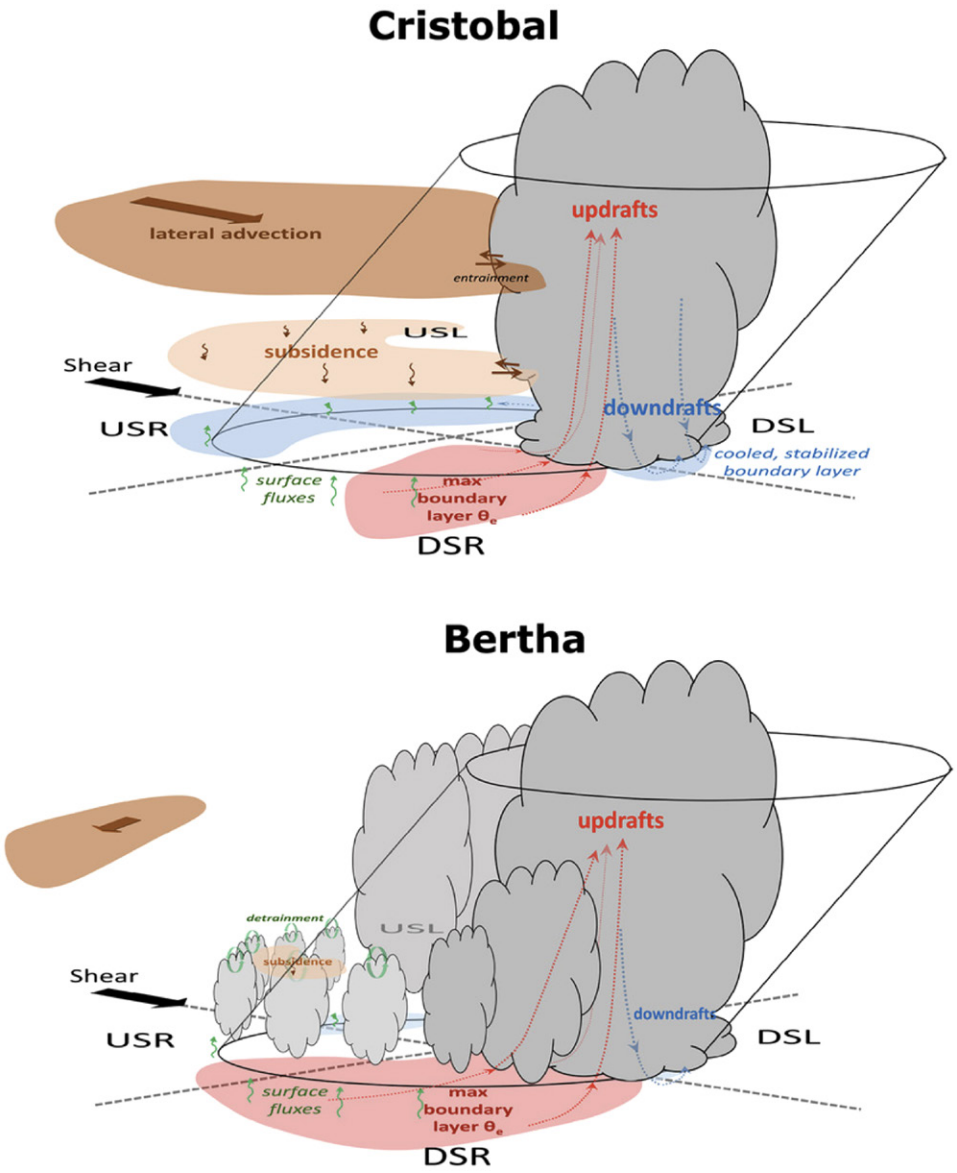

Fig. 9. Three-dimensional schematics summarizing hypothesized hindrances to precipitation symmetry in TCs in vertical wind shear (denoted by the black arrow in each panel). (top) An asymmetric case (Cristobal) and (bottom) a symmetric case (Bertha). The quadrants are denoted downshear right (DSR), downshear left (DSL), upshear left (USL), and upshear right (USR). Cloud features show locations of clouds and precipitation, and shading denotes regions of high (light red) and low (light blue) boundary layer θ_e. Dashed arrows denote updrafts (red) and downdrafts (blue). Green arrows show surface enthalpy fluxes; green circles in the bottom panel denote detrainment from clouds. Dark orange shading denotes lateral advection; light orange shading denotes mesoscale subsidence. Adapted from Nguyen et al. (2017).

characterized by high horizontal and vertical wind velocities, are likely ubiquitous in eyewalls of very intense TCs and that the strongest updrafts measured by dropwindsondes occur mainly to the left of the shear vector and in very intense, steady-state TCs; few occur in TCs that are undergoing rapid intensification. The strongest updraft and downdraft measured by dropwindsonde (27.4 and −30.1 m s^{-1}) were in Hurricanes Patricia and Felix at the time their rapid intensification had ended (Rogers et al. 2017; Aberson et al. 2017b). Moist entropy differences between the eye and eyewall show that advection from the eye to the eyewall can trigger intensification, especially in weak systems (Barnes and Fuentes 2010; Dolling and Barnes 2012), but the fact that the eye entropy is quickly depleted suggests that this process is rare. Strong eyewall downdrafts are not made up of low-entropy air, possibly because they

are associated with a large amount of evaporation; in contrast, weak downdrafts reaching the boundary layer are made of low-entropy air, suggesting that they are a greater hindrance to intensification than the strongest downdrafts (Wadler et al. 2018). TCs have some of the largest recorded helicity values, suggesting that supercells exist in TCs (Molinari and Vollaro 2008, 2010; Molinari et al. 2012). Baker et al. (2009) and Eastin and Link (2009) looked at whether midlatitude paradigms for supercells and tornadoes can be applied to landfalling TCs and found dry-air intrusions that affect the instability of mesoscale convective systems in TCs. TC intensity changes are related to the vertical motion in the eyewall (Lowag et al. 2008). Eastin et al. (2005a,b) documented the contribution of buoyant updrafts to the total upward mass transport using dropwindsonde and flight-level data. The low-level eye is an important source for buoyant updrafts in the eyewall via the export of high-entropy air, in addition to the low-level inflow from outside the TC. Most buoyant updrafts are located downshear left of the TC center, whereas convective downdraft cores are found upshear (Eastin et al. 2005a,b). Stern et al. (2016) found that the strongest low-level updrafts are not caused by buoyancy but agreed that they mainly occur to the left of the shear vector and in very intense, steady-state TCs.

Dropwindsonde observations led to great strides in identifying and understanding thermodynamic structures in both the large-scale tropical environment and within TCs themselves. Dunion and Velden (2004) used dropwindsonde data to show that the Jordan mean tropical sounding, said to represent the climatology in the tropical North Atlantic and Caribbean Sea, did not well represent the complex moisture distribution in the region, and new mean soundings for use in idealized models and other research were developed. Instead, a moist environment periodically modified by dry-air outbreaks from the Sahara and midlatitudes is evident. Forecast models were found to be too moist where there are Saharan air layers, and this bias can have a large impact on TC intensity and genesis forecasts (Zipser et al. 2009; Folmer et al. 2016).

Data from dropwindsondes released by high-altitude aircraft provided key insights into the structures of the upper-level outflow layer. Molinari et al. (2014) and Molinari and Vollaro (2014) found three turbulent layers associated with the upper-level outflow near the tropopause. The central dense overcast creates its own stability profile that influences the turbulence and the transition to outflow. Other upper-level sampling in a weak, sheared TC during the Fourth Convection and Moisture Experiment (CAMEX-4), especially within the eye, validated structures seen in mesoscale models (Halverson et al. 2006). The low surface pressure was accounted for by vertical layers of warming within the eye, and asymmetry was related to the interaction of the vortex with vertical wind shear. The observations confirmed model simulations and theory of sheared TCs (Heymsfield et al. 2006). Later high-altitude dropwindsonde data collected in six TCs during NASA's Hurricane and Severe Storm Sentinel experiment provided high-resolution observations of TC outflow and the warm core. The amplitude, but not the height, of the warm core was correlated with TC intensity. The outflow potential temperature was correlated with that of the low-level inflow rather than with TC intensity (Komaromi and Doyle 2017).

Dropwindsonde data have been critically important to the study of tropical cyclogenesis. Systems undergoing cyclogenesis have been sampled by aircraft far less frequently than developed TCs (Zawislak et al. 2022). Much of our current knowledge is from intensive airborne observing programs in 2006 [NASA's extension to the African Monsoon Multidisciplinary Analysis experiment (NAMMA; Zipser et al. 2009)] and 2010 [NASA's Genesis and Rapid Intensification Processes (GRIP; Braun et al. 2013) and the Pre-depression Investigation of Cloud Systems in the tropics (PREDICT) experiments; Montgomery et al. 2012]. Dropwindsonde data from NAMMA characterized waves as they emerged from the African coast and showed that those that develop into TCs exhibit small-amplitude midlevel troughs that were unlikely to

ingest dry, dusty Saharan air (Zawislak and Zipser 2010). Dropwindsonde data from PREDICT and GRIP showed that developing disturbances were moister than nondeveloping ones and that moisture and stability both increased with time; nondeveloping disturbances dried and become more unstable in time (Zawislak and Zipser 2014, Fig. 10). Vertical misalignment between low- and midlevel vortices made systems susceptible to dry-air entrainment (Davis and Ahijevych 2012, 2013; Komaromi 2013; Penny et al. 2015; Helms and Hart 2015; Brammer et al. 2018). Developing disturbances had large positive temperature anomalies that grew vertically and deepened, sometimes starting in the low to middle troposphere (Kerns and Chen 2015), and a strong upper-level radial temperature gradient. TC formation followed a path by which a midlevel vortex in a moist, humid environment precedes low-level vortex amplification (Davis et al. 2014; Zawislak and Zipser 2014). This pathway evolved such that the troposphere stabilizes (low-level cooling and upper-level warming), allowing the peak in the vertical mass flux to move to low altitudes (Raymond et al. 2011; Raymond and López Carrillo 2011). This process enhanced low-level mass convergence and vorticity, spinning up the vortex and suppressing lateral moisture export.

Dropwindsonde data have been used to study the end of the TC life cycle when they decay into remnant lows or transition into extratropical cyclones. Canada's Convair 580 aircraft conducted the first sampling of a TC undergoing extratropical transition in 2000. Abraham et al. (2004) and Fogarty et al. (2006) found a low-level stable layer over the cool ocean, large vertical gradients in horizontal wind speed, and a large area of strong low-level wind on the eastern side of the TC. They further used the data to validate numerical simulations. Dropwindsonde sampling and study of TCs undergoing extratropical transition is ongoing.

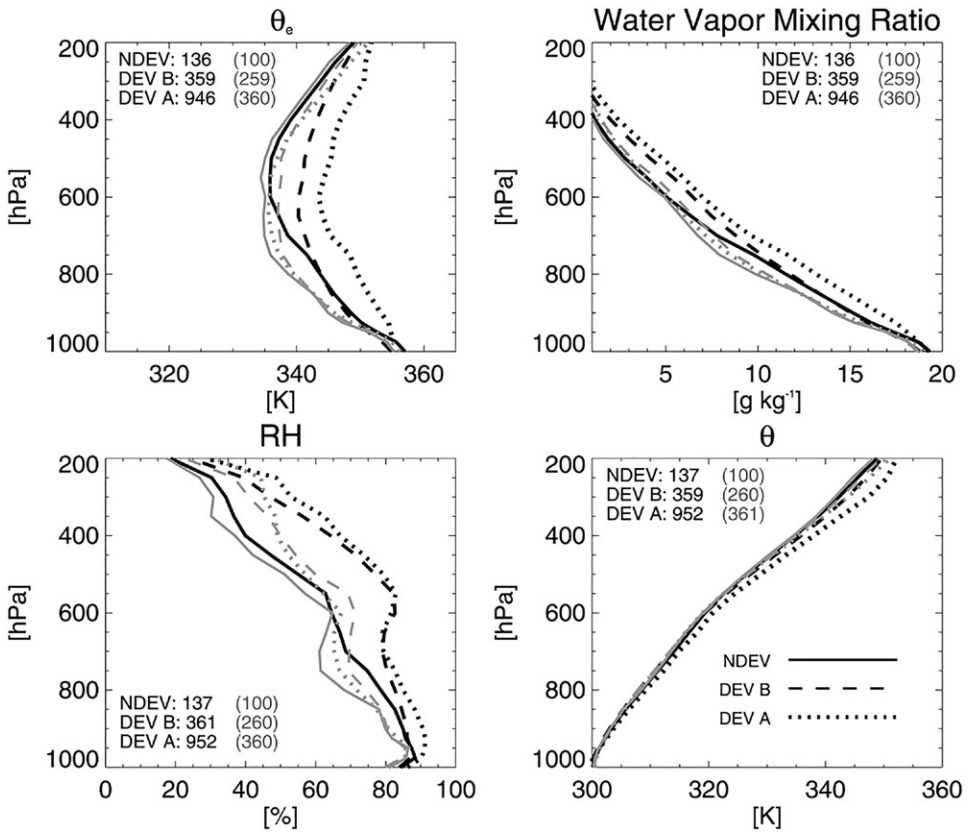

Fig. 10. Mean profiles of θ_e, water vapor mixing ratio (WVMR), relative humidity (RH), and potential temperature θ for nondeveloping (NDEV; solid), developing pregenesis (DEV B; dashed), and developing postgenesis (DEV A; dotted) cases. Profiles are separated for the core (within 333 km of the center; black) and environment (333–778 km of the center; gray). The approximate number of samples in each profile is in parentheses. From Zawislak and Zipser (2014).

The future

The impacts of GPS dropwindsonde data on TC climatology, forecasts, and understanding should not be underestimated. The dropwindsonde has provided researchers and operational scientists with accurate, high-resolution kinematic and thermodynamic observations since 1996. Observations in the turbulent boundary layer that were previously difficult to obtain have been especially important in improving physical parameterizations and numerical guidance. Improved physical understanding, advanced parameterization schemes, and enhanced data assimilation have resulted in improved forecasts and warnings. These improvements are summarized in this review.

The question now is, what's next? One change in the immediate future is to the instrument itself and the data that are transmitted. The NRD41 dropwindsonde will become the standard dropwindsonde during the 2023 hurricane season, and automatic launch mechanisms for this instrument are under development. Upgrades to aircraft-to-ground communications will allow for the transmission of the full high-resolution data in BUFR format to the ground allowing specialists to see small-scale features measured by the instruments and for the most data to be assimilated into model systems. And implementation of the IR sensor on all instruments to regularly measure sea surface temperature is possible.

Operational and research use of GPS dropwindsondes in TCs will continue for the foreseeable future, as they make up a vital part of the current mix of observations. One limitation of dropwindsondes is that they remain aloft for a limited time period with residence times for the instrument of about 5 min from the standard flight altitude inside the TC (~8–10 kft) and up to 20 min from high-altitude aircraft (>40 kft); the residence time is only about 1 min within the boundary layer. Innovations using AVAPS can help to solve this problem. Small Uncrewed Aerial Systems (sUASs) may allow for anywhere between 1.5 and 4 h of residence time within the boundary layer, increasing the total number of observations and expanding coverage within the TC. The sUASs will be able to measure sea surface temperature using an onboard IR sensor, wave height/spectra via altimetry, and high-frequency wind velocity using multihole probes, allowing for direct momentum-flux measurements using an eddy correlation method. It is worth noting that the sUAS's IR/SST capability can be incorporated onto the existing dropwindsonde platform for minimal cost and engineering outlay. Coyote sUAS flights in major Hurricanes Edouard, Maria, and Michael (Cione et al. 2020) and an Altius 600[3] flight into major Hurricane Ian suggest that the future is bright for this emerging technology.

[3] Information on the Altius 600 can be found at https://areai.com/altius-600-2/.

Other potential technologies that could increase the volumetric and temporal coverage of observations within TC environments are Skyfora's StreamSonde and WindBorne balloons. StreamSonde is a promising air-deployed observing system that could provide valuable data using a swarm of very light, small sensors that stay aloft and transmit data for 30–60 min or longer. This will be tested in clear air by NOAA in 2023 and remains as an intriguing possibility to explore in TC environments in the future. WindBorne, a potentially global constellation of low-cost, long-duration (on the order of 1–2 weeks), weather balloons that can be deployed from land, sea, and air, can provide observations throughout the troposphere. This system was tested using land-based deployments during the 2022 Atlantic Hurricane season. A major focus of the Advancing the Prediction of Hurricanes Experiment (APHEX; Zawislak et al. 2022) is to explore new observing systems, and other encouraging technologies are in development. NOAA and its partner organizations will continue to investigate and invest in the most promising examples of these new emerging systems as they become available.

Acknowledgments. The authors thank Trey Alvey, Frank Marks, James Franklin, Holger Vömel, and an anonymous reviewer for helpful comments on various versions of the manuscript. Mike Jankulak helped edit the manuscript. Jun Zhang acknowledges support from NOAA Grants

NA21OAR4590370, NA22OAR4590118, and NA22OAR4590178; NSF Grant AGS2211308; and ONR Grant N00014-20-1-2071. Jonathan Zawislak acknowledges support from NASA Grant 80NSSC19K0012 under the Weather and Atmospheric Dynamics program and TCRI ONR BAA N00014-19-S-B001. Kathryn Sellwood acknowledges funding from TCRI ONR BAA N00014-19-S-B001. The scientific results and conclusions, as well as any views or opinions expressed herein, are those of the author(s) and do not necessarily reflect those of OAR or the Department of Commerce.

Data availability statement. No datasets were generated or analyzed during the current study. A continuously updated dropwindsonde data archive in and around TCs is maintained by AOML/HRD. The data are organized by year, storm name, and aircraft mission and are available at https://www.aoml.noaa.gov/data-products/#hurricanedata, with information on the data formats at https://www.aoml.noaa.gov/hrd/Storm_pages/sondeformat.html.

References

Abarca, S. F., M. T. Montgomery, S. A. Braun, and J. Dunion, 2016: On the secondary eyewall formation of Hurricane Edouard (2014). *Mon. Wea. Rev.*, **144**, 3321–3331, https://doi.org/10.1175/MWR-D-15-0421.1.

Aberson, S. D., 2002: Two years of operational hurricane synoptic surveillance. *Wea. Forecasting*, **17**, 1101–1110, https://doi.org/10.1175/1520-0434(2002)017<1101:TYOOHS>2.0.CO;2.

——, 2003: Targeted observations to improve operational tropical cyclone track forecast guidance. *Mon. Wea. Rev.*, **131**, 1613–1628, https://doi.org/10.1175//2550.1.

——, 2008: Large forecast degradations due to synoptic surveillance during the 2004 and 2005 hurricane seasons. *Mon. Wea. Rev.*, **136**, 3138–3150, https://doi.org/10.1175/2007MWR2192.1.

——, 2010: 10 years of hurricane synoptic surveillance (1997–2006). *Mon. Wea. Rev.*, **138**, 1536–1549, https://doi.org/10.1175/2009MWR3090.1.

——, and J. L. Franklin, 1999: Impact on hurricane track and intensity forecasts of GPS dropwindsonde observations from the first-season flights of the NOAA Gulfstream-IV jet aircraft. *Bull. Amer. Meteor. Soc.*, **80**, 421–428, https://doi.org/10.1175/1520-0477(1999)080<0421:IOHTAI>2.0.CO;2.

——, and B. J. Etherton, 2006: Targeting and data assimilation studies during Hurricane Humberto (2001). *J. Atmos. Sci.*, **62**, 175–186, https://doi.org/10.1175/JAS3594.1.

——, M. T. Montgomery, M. M. Bell, and M. L. Black, 2006: Hurricane Isabel (2003): New insights into the physics of intense storms. Part II: Extreme localized wind. *Bull. Amer. Meteor. Soc.*, **87**, 1349–1354, https://doi.org/10.1175/BAMS-87-10-1349.

——, K. J. Sellwood, and P. A. Leighton, 2017a: Calculating dropwindsonde location and time from TEMP-DROP messages for accurate assimilation and analysis. *J. Atmos. Oceanic Technol.*, **34**, 1673–1678, https://doi.org/10.1175/JTECH-D-17-0023.1.

——, J. A. Zhang, and K. N. Ocasio, 2017b: An extreme event in the eyewall of Hurricane Felix on 2 September 2007. *Mon. Wea. Rev.*, **145**, 2083–2092, https://doi.org/10.1175/MWR-D-16-0364.1.

Abraham, J., J. W. Strapp, C. Fogarty, and M. Wolde, 2004: Extratropical transition of Hurricane Michael: An aircraft investigation. *Bull. Amer. Meteor. Soc.*, **85**, 1323–1339, https://doi.org/10.1175/BAMS-85-9-1323.

Ancell, B., and G. J. Hakim, 2007: Comparing adjoint and ensemble sensitivity analysis with applications to observation targeting. *Mon. Wea. Rev.*, **135**, 4117–4134, https://doi.org/10.1175/2007MWR1904.1.

Baker, A. K., M. D. Parker, and M. D. Eastin, 2009: Environmental ingredients for supercell and tornadoes within Hurricane Ivan. *Wea. Forecasting*, **24**, 223–244, https://doi.org/10.1175/2008WAF2222146.1.

Barnes, G. M., 2008: Atypical thermodynamic profiles in hurricanes. *Mon. Wea. Rev.*, **136**, 631–643, https://doi.org/10.1175/2007MWR2033.1.

——, and P. Fuentes, 2010: Eye excess energy and the rapid intensification of Hurricane Lili (2002). *Mon. Wea. Rev.*, **138**, 1446–1458, https://doi.org/10.1175/2009MWR3145.1.

——, and K. P. Dolling, 2013: The inflow to tropical Cyclone Humberto (2001) as viewed with azimuth–height surfaces over three days. *Mon. Wea. Rev.*, **141**, 1324–1336, https://doi.org/10.1175/MWR-D-11-00348.1.

Bell, M. M., and M. T. Montgomery, 2008: Observed structure, evolution, and potential intensity of category 5 Hurricane Isabel (2003) from 12 to 14 September. *Mon. Wea. Rev.*, **136**, 2023–2046, https://doi.org/10.1175/2007MWR1858.1.

——, ——, and K. A. Emanuel, 2012: Air-sea enthalpy and momentum exchange at major hurricane wind speeds observed during CBLAST. *J. Atmos. Sci.*, **69**, 3197–3222, https://doi.org/10.1175/JAS-D-11-0276.1.

Black, P. L., L. Harrison, M. Beaubien, R. Bluth, R. Woods, A. Penny, R. W. Smith, and J. D. Doyle, 2017: High-Definition Sounding System (HDSS) for atmospheric profiling. *J. Atmos. Oceanic Technol.*, **34**, 777–796, https://doi.org/10.1175/JTECH-D-14-00210.1.

Brammer, A., C. D. Thorncroft, and J. P. Dunion, 2018: Observations and predictability of a nondeveloping tropical disturbance of the eastern Atlantic. *Mon. Wea. Rev.*, **146**, 3079–3096, https://doi.org/10.1175/MWR-D-18-0065.1.

Braun, S. A., and Coauthors, 2013: NASA's Genesis and Rapid Intensification Processes (GRIP) field experiment. *Bull. Amer. Meteor. Soc.*, **94**, 345–363, https://doi.org/10.1175/BAMS-D-11-00232.1.

——, P. A. Newman, and G. M. Heymsfield, 2016: NASA's Hurricane and Severe Storm Sentinel (HS3) investigation. *Bull. Amer. Meteor. Soc.*, **97**, 2085–2102, https://doi.org/10.1175/BAMS-D-15-00186.1.

Brown, R. A., and L. Zeng, 2002: Comparison of boundary layer model winds with dropsonde observations in tropical cyclones. *J. Appl. Meteor.*, **40**, 1718–1723, https://doi.org/10.1175/1520-0450(2001)040<1718:COPBLM>2.0.CO;2.

Bryan, G. H., R. P. Worsnop, J. K. Lundquist, and J. A. Zhang, 2017: A simple method for simulating wind profiles in the boundary layer of tropical cyclones. *Bound.-Layer Meteor.*, **162**, 475–502, https://doi.org/10.1007/s10546-016-0207-0.

Bucci, L. R., C. O'Handley, G. D. Emmitt, J. A. Zhang, K. Ryan, and R. Atlas, 2018: Validation of an airborne Doppler wind lidar in tropical cyclones. *Sensors*, **18**, 4288, https://doi.org/10.3390/s18124288.

Burpee, R. W., D. G. Marks, and R. T. Merrill, 1984: An assessment of omega dropwindsonde data in track forecasts of Hurricane Debby (1982). *Bull. Amer. Meteor. Soc.*, **65**, 1050–1058, https://doi.org/10.1175/1520-0477(1984)065<1050:AAOODD>2.0.CO;2.

——, J. L. Franklin, S. J. Lord, R. E. Tuleya, and S. D. Aberson, 1996: The impact of omega dropwindsondes on operational hurricane track forecast models. *Bull. Amer. Meteor. Soc.*, **77**, 925–934, https://doi.org/10.1175/1520-0477(1996)077<0925:TIOODO>2.0.CO;2.

Chen, S.-H., 2007: The impact of assimilating SSM/I and QuikSCAT satellite winds on Hurricane Isidore simulations. *Mon. Wea. Rev.*, **135**, 549–566, https://doi.org/10.1175/MWR3283.1.

Chou, K.-H., and C.-C. Wu, 2008: Typhoon initialization in a mesoscale model – Combination of the bogus vortex and the dropwindsonde data in DOTSTAR. *Mon. Wea. Rev.*, **136**, 865–879, https://doi.org/10.1175/2007MWR2141.1.

——, ——, P.-H. Lin, and S. Majumdar, 2010: Validation of QuikSCAT wind vectors by dropwindsonde data from Dropwindsonde Observations for Typhoon Surveillance near the Taiwan Region (DOTSTAR). *J. Geophys. Res.*, **115**, D02109, https://doi.org/10.1029/2009JD012131.

Chou, K.-S., C.-C. Wu, P.-H. Lin, S. D. Aberson, M. Weissmann, F. Harnisch, and T. Nakazawa, 2011: The impact of dropwindsonde observations on typhoon track forecasts in DOTSTAR and T-PARC. *Mon. Wea. Rev.*, **139**, 1728–1743, https://doi.org/10.1175/2010MWR3582.1.

Christophersen, H., A. Aksoy, P. Dunion, and K. Sellwood, 2017: The impact of NASA Global Hawk unmanned aircraft dropwindsonde observations on tropical cyclone track, intensity and structure: Case studies. *Mon. Wea. Rev.*, **145**, 1817–1830, https://doi.org/10.1175/MWR-D-16-0332.1.

——, ——, J. Dunion, and S. Aberson, 2018a: Composite impact of Global Hawk unmanned aircraft dropwindsondes on tropical cyclone analyses and forecasts. *Mon. Wea. Rev.*, **146**, 2297–2314, https://doi.org/10.1175/MWR-D-17-0304.1.

——, R. Atlas, A. Aksoy, and J. Dunion, 2018b: Combined use of satellite observations and Global Hawk unmanned aircraft dropwindsondes for improved tropical cyclone analyses and forecasts. *Wea. Forecasting*, **33**, 1021–1031, https://doi.org/10.1175/WAF-D-17-0167.1.

Cione, J. J., E. Kalina, E. Uhlhorn, and A. Damiano, 2016: Coyote unmanned aircraft system observations in Hurricane Edouard (2014). *Earth Space Sci.*, **3**, 370–380, https://doi.org/10.1002/2016EA000187.

——, and Coauthors, 2020: Eye of the storm: Observing hurricanes with a small unmanned aircraft system. *Bull. Amer. Meteor. Soc.*, **101**, E186–E205, https://doi.org/10.1175/BAMS-D-19-0169.1.

Dabberdt, W., H. Cole, A. Paukkunen, J. Horhammer, V. Antikainen, and R. Shellhorn, 2022: Radiosondes. *Encyclopedia of Atmospheric Sciences*, Vol. 6, J. R. Holton, J. Pyle, and J. A. Curry, Eds., Academic Press, 1900–1913.

Davis, C. A., and D. A. Ahijevych, 2012: Mesoscale structural evolution of three tropical weather systems observed during PREDICT. *J. Atmos. Sci.*, **69**, 1284–1305, https://doi.org/10.1175/JAS-D-11-0225.1.

——, and ——, 2013: Thermodynamic environments of deep convection in Atlantic tropical disturbances. *J. Atmos. Sci.*, **70**, 1912–1928, https://doi.org/10.1175/JAS-D-12-0278.1.

——, A. David, J. A. Haggerty, and M. J. Mahoney, 2014: Observations of temperature in the upper troposphere and lower stratosphere of tropical weather disturbances. *J. Atmos. Sci.*, **71**, 1593–1608, https://doi.org/10.1175/JAS-D-13-0278.1.

Delgado, S., C. W. Landsea, and H. Willoughby, 2018: Reanalysis of the 1954–63 Atlantic hurricane seasons. *J. Climate*, **32**, 4177–4192, https://doi.org/10.1175/JCLI-D-15-0537.1.

Ditchek, S. D., and J. A. Sippel, 2023: A comparison of the impacts of inner-core, in-vortex, and environmental dropsondes on tropical cyclone forecasts during the 2017–20 hurricane seasons. *Wea. Forecasting*, **38**, 2169–2187, https://doi.org/10.1175/WAF-D-23-0055.1.

Dolling, K. P., and G. M. Barnes, 2012: The creation of a high equivalent potential temperature reservoir in Tropical Storm Humberto (2001) and its possible role in storm deepening. *Mon. Wea. Rev.*, **140**, 492–50, https://doi.org/10.1175/MWR-D-11-00068.1.

Dunion, J. P., and C. S. Velden, 2002: Application of surface-adjusted GOES low-level cloud-drift winds in the environment of Atlantic tropical cyclones. Part I: Methodology and validation. *Mon. Wea. Rev.*, **130**, 1333–1346, https://doi.org/10.1175/1520-0493(2002)130<1333:AOSAGL>2.0.CO;2.

——, and ——, 2004: The impact of the Saharan air layer on Atlantic tropical cyclone activity. *Bull. Amer. Meteor. Soc.*, **85**, 353–365, https://doi.org/10.1175/BAMS-85-3-353.

——, S. H. Houston, C. S. Velden, and M. D. Powell, 2002: Application of surface-adjusted GOES low-level cloud-drift winds in the environment of Atlantic tropical cyclones. Part II: Integration into surface wind analyses. *Mon. Wea. Rev.*, **130**, 1347–1355, https://doi.org/10.1175/1520-0493(2002)130<1347:AOSAGL>2.0.CO;2.

——, C. W. Landsea, S. H. Houston, and M. D. Powell, 2003: A reanalysis of the surface winds for Hurricane Donna of 1960. *Mon. Wea. Rev.*, **131**, 1992–2011, https://doi.org/10.1175/1520-0493(2003)131<1992:AROTSW>2.0.CO;2.

Eastin, M. D., and M. C. Link, 2009: Miniature supercells in an offshore outer rainband of Hurricane Ivan (2004). *Mon. Wea. Rev.*, **137**, 2081–2104, https://doi.org/10.1175/2009MWR2753.1.

——, W. M. Gray, and P. G. Black, 2005a: Buoyancy of convective vertical motions in the inner core of intense hurricanes. Part I: General statistics. *Mon. Wea. Rev.*, **133**, 188–208, https://doi.org/10.1175/MWR-2848.1.

——, ——, and ——, 2005b: Buoyancy of convective vertical motions in the inner core of intense hurricanes. Part II: Case studies. *Mon. Wea. Rev.*, **133**, 209–227, https://doi.org/10.1175/MWR-2849.1.

Fogarty, C. T., R. J. Greatbatch, and H. Ritchie, 2006: The role of anomalously warm sea surface temperatures on the intensity of Hurricane Juan (2003) during its approach to Nova Scotia. *Mon. Wea. Rev.*, **134**, 1484–1504, https://doi.org/10.1175/MWR3140.1.

Folmer, M. J., R. W. Pasken, S. Chiao, J. Dunion, and J. Halverson, 2016: Modeling studies on the formation of Hurricane Helene: The impact of GPS dropwindsondes from the NAMMA 2006 field campaign. *Meteor. Atmos. Phys.*, **128**, 733–750, https://doi.org/10.1007/s00703-016-0452-2.

Franklin, J. L., and P. R. Julian, 1985: An investigation of Omega windfinding accuracy. *J. Atmos. Oceanic Technol.*, **2**, 212–231, https://doi.org/10.1175/1520-0426(1985)002<0212:AIOOWA>2.0.CO;2.

——, and M. DeMaria, 1992: The impact of Omega dropwindsonde observations on barotropic hurricane track forecasts. *Mon. Wea. Rev.*, **120**, 381–391, https://doi.org/10.1175/1520-0493(1992)120<0381:TIOODO>2.0.CO;2.

——, M. L. Black, and K. Valde, 2003: GPS dropwindsonde wind profiles in hurricanes and their operational implications. *Wea. Forecasting*, **18**, 32–44, https://doi.org/10.1175/1520-0434(2003)018<0032:GDWPIH>2.0.CO;2.

French, J. R., W. M. Drennan, J. A. Zhang, and P. G. Black, 2007: Turbulent fluxes in the hurricane boundary layer. Part I: Momentum flux. *J. Atmos. Sci.*, **64**, 1089–1102, https://doi.org/10.1175/JAS3887.1.

Gao, Y., C. Guan, J. Sun, and L. Xie, 2018: A new hurricane wind direction retrieval method for SAR images without hurricane eye. *J. Atmos. Oceanic Technol.*, **35**, 2229–2239, https://doi.org/10.1175/JTECH-D-18-0053.1.

Giammanco, I. M., J. L. Schroeder, and M. D. Powell, 2013: GPS dropwindsonde and WSR-88D observations of tropical cyclone vertical wind profiles and their characteristics. *Wea. Forecasting*, **28**, 77–99, https://doi.org/10.1175/WAF-D-11-00155.1.

Govind, P. K., 1975: Dropwindsonde instrumentation for weather reconnaissance aircraft. *J. Appl. Meteor.*, **14**, 1512–1520, https://doi.org/10.1175/1520-0450(1975)014<1512:DIFWRA>2.0.CO;2.

Griffin, J. S., R. W. Burpee, F. D. Marks, and J. L. Franklin, 1992: Real-time airborne analysis of aircraft data supporting operational hurricane forecasting. *Wea. Forecasting*, **7**, 480–490, https://doi.org/10.1175/1520-0434(1992)007<0480:RTAAOA>2.0.CO;2.

Hagen, A. B., D. Strahan-Sakoskie, and C. Luckett, 2012: A reanalysis of the 1944–53 Atlantic hurricane seasons – The first decade of aircraft reconnaissance. *J. Climate*, **25**, 4441–4460, https://doi.org/10.1175/JCLI-D-11-00419.1.

Halverson, J. B., J. Simpson, G. Heymsfield, H. Pierce, T. Hock, and L. Ritchie, 2006: Warm core structure of Hurricane Erin diagnosed from high altitude dropsondes during CAMEX-4. *J. Atmos. Sci.*, **63**, 309–324, https://doi.org/10.1175/JAS3596.1.

Helms, C. N., and R. E. Hart, 2015: The evolution of dropsonde-derived kinematic and thermodynamic structure in developing and non developing Atlantic tropical convective systems. *Mon. Wea. Rev.*, **143**, 3109–3135, https://doi.org/10.1175/MWR-D-14-00242.1.

Heymsfield, G. M., J. Halverson, E. Ritchie, J. Simpson, J. Molinari, and L. Tian, 2006: Structure of highly sheared Tropical Storm Chantal during CAMEX-4. *J. Atmos. Sci.*, **63**, 268–287, https://doi.org/10.1175/JAS3602.1.

Hock, T. F., and J. L. Franklin, 1999: The NCAR GPS dropwindsonde. *Bull. Amer. Meteor. Soc.*, **80**, 407–420, https://doi.org/10.1175/1520-0477(1999)080<0407:TNGD>2.0.CO;2.

Holbach, H. M., E. W. Uhlhorn, and M. A. Bourassa, 2018: Off-nadir SFMR brightness temperature measurements in high-wind conditions. *J. Atmos. Oceanic Technol.*, **35**, 1865–1879, https://doi.org/10.1175/JTECH-D-18-0005.1.

Holt, C., I. Szunyogh, G. Gyarmati, S. M. Leidner, and R. N. Hoffman, 2015: Assimilation of tropical cyclone observations: Improving the assimilation of TCVitals, scatterometer winds, and dropwindsonde observations. *Mon. Wea. Rev.*, **143**, 3956–3980, https://doi.org/10.1175/MWR-D-14-00158.1.

Holthuijsen, L. H., M. D. Powell, and J. D. Pietrzak, 2012: Wind and waves in extreme hurricanes. *J. Geophys. Res.*, **117**, C09003, https://doi.org/10.1029/2012JC007983.

Kaisti, K., 1995: New low-cost GPS solution for upper air wind. Preprints, *Ninth Symp. on Meteorological Observations and Instrumentation*, Charlotte, NC, Amer. Meteor. Soc., 16–20.

Kamineni, R., T. N. Krishnamurti, S. Pattnaik, E. V. Browell, S. Ismail, and R. A. Ferrare, 2006: Impact of CAMEX-4 datasets for hurricane forecasts using a global model. *J. Atmos. Sci.*, **63**, 151–174, https://doi.org/10.1175/JAS3588.1.

Kepert, J., 2001: The dynamics of boundary layer jets in the tropical cyclone core. Part I: Linear theory. *J. Atmos. Sci.*, **58**, 2469–2484, https://doi.org/10.1175/1520-0469(2001)058<2469:TDOBLJ>2.0.CO;2.

——, 2006a: Observed boundary layer wind structure and balance in the Hurricane Core. Part I: Hurricane Georges. *J. Atmos. Sci.*, **63**, 2169–2193, https://doi.org/10.1175/JAS3745.1.

——, 2006b: Observed boundary layer wind structure and balance in the Hurricane Core. Part II: Hurricane Mitch. *J. Atmos. Sci.*, **63**, 2194–2211, https://doi.org/10.1175/JAS3746.1.

——, and Y. Wang, 2002: The dynamics of boundary layer jets within the tropical cyclone core. Part II: Nonlinear enhancement. *J. Atmos. Sci.*, **58**, 2485–2501, https://doi.org/10.1175/1520-0469(2001)058<2485:TDOBLJ>2.0.CO;2.

Kerns, B. W., and S. S. Chen, 2015: Subsidence warming as an under appreciated ingredient in tropical cyclogenesis. Part I: Aircraft observations. *J. Atmos. Sci.*, **72**, 4237–4260, https://doi.org/10.1175/JAS-D-14-0366.1.

Kieper, M. E., C. W. Landsea, and J. L. Beven, 2016: A reanalysis of Hurricane Camille. *Bull. Amer. Meteor. Soc.*, **97**, 367–384, https://doi.org/10.1175/BAMS-D-14-00137.1.

Klotz, B. W., and E. W. Uhlhorn, 2014: Improved stepped frequency microwave radiometer tropical cyclone surface winds in heavy precipitation. *J. Atmos. Oceanic Technol.*, **31**, 2392–2408, https://doi.org/10.1175/JTECH-D-14-00028.1.

Komaromi, W. A., 2013: An investigation of composite dropsonde profiles for developing and nondeveloping tropical waves during the 2010 PREDICT field campaign. *J. Atmos. Sci.*, **70**, 542–558, https://doi.org/10.1175/JAS-D-12-052.1.

——, and J. D. Doyle, 2017: Tropical cyclone outflow and warm core structure as revealed by HS3 dropsonde data. *Mon. Wea. Rev.*, **145**, 1339–1359, https://doi.org/10.1175/MWR-D-16-0172.1.

Kren, A. C., L. Cucurull, and H. Wang, 2018: Impact of UAS Global Hawk dropsonde data on tropical and extratropical cyclone forecasts in 2016. *Wea. Forecasting*, **33**, 1121–1141, https://doi.org/10.1175/WAF-D-18-0029.1.

Landsea, C. W., and Coauthors, 2004: A reanalysis of Hurricane Andrew's intensity. *Bull. Amer. Meteor. Soc.*, **85**, 1699–1712, https://doi.org/10.1175/BAMS-85-11-1699.

——, and Coauthors, 2008: A reanalysis of the 1911–20 Atlantic hurricane database. *J. Climate*, **21**, 2138–2168, https://doi.org/10.1175/2007JCLI1119.1.

——, S. Feuer, A. Hagen, D. A. Glenn, J. Sims, R. Perez, M. Chenoweth, and N. Anderson, 2012: A reanalysis of the 1921–30 Atlantic hurricane database. *J. Climate*, **25**, 865–885, https://doi.org/10.1175/JCLI-D-11-00026.1.

——, A. Hagen, W. Bredemeyer, C. Carrasco, D. A. Glenn, A. Santiago, D. Strahan-Sakoskie, and M. Dickinson, 2014: A reanalysis of the 1931 to 1943 Atlantic hurricane database. *J. Climate*, **27**, 6093–6118, https://doi.org/10.1175/JCLI-D-13-00503.1.

Lawrence, M. B., 1999: Eastern North Pacific hurricane season of 1997. *Mon. Wea. Rev.*, **127**, 2440–2454, https://doi.org/10.1175/1520-0493(1999)127<2440:ENPHSO>2.0.CO;2.

Lee, C.-Y., and S. S. Chen, 2012: Symmetric and asymmetric structures of hurricane boundary layer in coupled atmosphere-wave-ocean models and observations. *J. Atmos. Sci.*, **69**, 3576–3594, https://doi.org/10.1175/JAS-D-12-046.1.

Liu, Z., C. S. Schwartz, C. Snyder, and S.-Y. Ha, 2012: Impact of assimilating AMSU-A radiances on forecasts of 2008 Atlantic tropical cyclones initialized with a limited-area ensemble Kalman filter. *Mon. Wea. Rev.*, **140**, 4017–4034, https://doi.org/10.1175/MWR-D-12-00083.1.

Lowag, A., M. L. Black, and M. D. Eastin, 2008: Structural and intensity changes of Hurricane Bret (1999). Part I: Environmental influences. *Mon. Wea. Rev.*, **136**, 4320–4333, https://doi.org/10.1175/2008MWR2438.1.

Majumdar, S. J., M. J. Brennan, and K. Howard, 2013: The impact of dropwindsonde and supplemental rawinsonde observations on track forecasts for Hurricane Irene (2011). *Wea. Forecasting*, **28**, 1385–1403, https://doi.org/10.1175/WAF-D-13-00018.1.

Ming, J., J. A. Zhang, and R. F. Rogers, 2015: Typhoon kinematic and thermodynamic boundary layer structure from dropsonde composites. *J. Geophys. Res. Atmos.*, **120**, 3158–3172, https://doi.org/10.1002/2014JD022640.

Molinari, J., and D. Vollaro, 2008: Extreme helicity and intense convective towers in Hurricane Bonnie. *Mon. Wea. Rev.*, **136**, 4355–4372, https://doi.org/10.1175/2008MWR2423.1.

——, and ——, 2010: Distribution of helicity, CAPE, and shear in tropical cyclones. *J. Atmos. Sci.*, **67**, 274–284, https://doi.org/10.1175/2009JAS3090.1.

——, and ——, 2014: Symmetric instability in the outflow layer of a major hurricane. *J. Atmos. Sci.*, **71**, 3739–3746, https://doi.org/10.1175/JAS-D-14-0117.1.

——, D. M. Romps, D. Vollaro, and L. Nguyen, 2012: CAPE in tropical cyclones. *J. Atmos. Sci.*, **69**, 2452–2463, https://doi.org/10.1175/JAS-D-11-0254.1.

——, P. Duran, and D. Vollaro, 2014: Low Richardson number in the tropical cyclone outflow layer. *J. Atmos. Sci.*, **71**, 3164–3179, https://doi.org/10.1175/JAS-D-14-0005.1.

Montgomery, M. T., M. M. Bell, S. D. Aberson, and M. L. Black, 2006: Hurricane Isabel (2003): New insights into the physics of intense storms. Part I: Mean vortex structure and maximum intensity estimates. *Bull. Amer. Meteor. Soc.*, **87**, 1335–1347, https://doi.org/10.1175/BAMS-87-10-1335.

——, and Coauthors, 2012: The Pre-Depression Investigation of Cloud Systems in the Tropics (PREDICT) experiment: Scientific basis, new analysis tools and some first results. *Bull. Amer. Meteor. Soc.*, **93**, 153–172, https://doi.org/10.1175/BAMS-D-11-00046.1.

——, J. A. Zhang, and R. K. Smith, 2014: An analysis of the observed low-level structure of rapidly intensifying and mature Hurricane Earl (2010). *Quart. J. Roy. Meteor. Soc.*, **140**, 2132–2146, https://doi.org/10.1002/qj.2283.

Nguyen, L. T., R. F. Rogers, and P. D. Reasor, 2017: Thermodynamic and kinematic influences on precipitation symmetry in sheared tropical cyclones: Bertha and Cristobal (2014). *Mon. Wea. Rev.*, **145**, 4423–4446, https://doi.org/10.1175/MWR-D-17-0073.1.

——, ——, J. A. Zawislak, and J. A. Zhang, 2019: Assessing the influence of convective downdrafts and surface enthalpy fluxes on tropical cyclone intensity change in moderate vertical wind shear. *Mon. Wea. Rev.*, **147**, 3519–3534, https://doi.org/10.1175/MWR-D-18-0461.1.

Nugent, A. D., and R. Rios-Berrios, 2018: Factors leading to extreme precipitation on Dominica from Tropical Storm Erika (2015). *Mon. Wea. Rev.*, **146**, 525–541, https://doi.org/10.1175/MWR-D-17-0242.1.

Pasch, R. J., L. A. Avila, and J. L. Guiney, 2001: Atlantic hurricane season of 1998. *Mon. Wea. Rev.*, **129**, 3085–3123, https://doi.org/10.1175/1520-0493(2001)129<3085:AHSO>2.0.CO;2.

Penny, A. B., P. A. Harr, and M. M. Bell, 2015: Observations of a non developing tropical disturbance in the western North Pacific during TCS-08 (2008). *Mon. Wea. Rev.*, **143**, 2459–2484, https://doi.org/10.1175/MWR-D-14-00163.1.

Powell, M. D., P. J. Vickery, and T. A. Reinhold, 2003: Reduced drag coefficient for high wind speeds in tropical cyclones. *Nature*, **422**, 279–283, https://doi.org/10.1038/nature01481.

——, E. W. Uhlhorn, and J. D. Kepert, 2009: Estimating maximum surface winds from hurricane reconnaissance measurements. *Wea. Forecasting*, **24**, 868–883, https://doi.org/10.1175/2008WAF2007087.1.

Press, W. H., S. A. Teukolsky, W. T. Vetterling, and B. P. Flannery, 2007: *Numerical Recipes: The Art of Scientific Computing.* 3rd ed. Cambridge University Press, 1256 pp.

Raymond, D. J., and C. López Carrillo, 2011: Vorticity budget of typhoon Nuri. *Atmos. Chem. Phys.*, **11**, 147–163, https://doi.org/10.5194/acp-11-147-2011.

——, S. L. Sessions, and C. López Carillo, 2011: Thermodynamics of tropical cyclogenesis in the northwest Pacific. *J. Geophys. Res.*, **116**, D18101, https://doi.org/10.1029/2011JD015624.

Reynolds, C. A., J. D. Doyle, R. M. Hodur, and H. Jin, 2010: Naval Research Laboratory multiscale targeting guidance for T-PARC and TCS-08. *Wea. Forecasting*, **25**, 526–544, https://doi.org/10.1175/2009WAF2222292.1.

——, R. Langland, P. M. Pauley, and C. Velden, 2013: Tropical cyclone data impact studies: Influence of model bias and synthetic observations. *Mon. Wea. Rev.*, **141**, 4373–4394, https://doi.org/10.1175/MWR-D-12-00300.1.

Richter, D. H., and D. P. Stern, 2014: Evidence of spray-mediated enthalpy flux within tropical cyclones. *Geophys. Res. Lett.*, **41**, 2997–3003, https://doi.org/10.1002/2014GL059746.

——, R. Bohac, and D. P. Stern, 2016: An assessment of the flux profile method for determining air–sea momentum and enthalpy fluxes from dropsonde data in tropical cyclones. *J. Atmos. Sci.*, **73**, 2665–2682, https://doi.org/10.1175/JAS-D-15-0331.1.

——, C. Wainwright, D. P. Stern, G. H. Bryan, and D. Chavas, 2021: Potential low bias in high-wind drag coefficient inferred from dropsonde data in hurricanes. *J. Atmos. Sci.*, **78**, 2339–2352, https://doi.org/10.1175/JAS-D-20-0390.1.

Rios-Berrios, R., and R. D. Torn, 2017: Climatological analysis of tropical cyclone intensity changes under moderate vertical wind shear. *Mon. Wea. Rev.*, **145**, 1717–1738, https://doi.org/10.1175/MWR-D-16-0350.1.

Rogers, R. F., P. D. Reasor, and J. A. Zhang, 2015: Multiscale structure and evolution of Hurricane Earl (2010) during rapid intensification. *Mon. Wea. Rev.*, **143**, 536–562, https://doi.org/10.1175/MWR-D-14-00175.1.

——, J. A. Zhang, J. Zawislak, G. R. Alvey III, E. J. Zipser, and S. N. Stevenson, 2016: Observations of the structure and evolution of Hurricane Edouard (2014) during intensity change. Part II: Kinematic structure and the distribution of deep convection. *Mon. Wea. Rev.*, **144**, 3355–3376, https://doi.org/10.1175/MWR-D-16-0017.1.

——, S. Aberson, M. M. Bell, D. J. Cecil, J. D. Doyle, J. Morgerman, L. K. Shay, and C. Velden, 2017: Rewriting the tropical record books: The extraordinary intensification of Hurricane Patricia (2015). *Bull. Amer. Meteor. Soc.*, **98**, 2091–2112, https://doi.org/10.1175/BAMS-D-16-0039.1.

——, P. D. Reasor, J. T. Zawislak, and L. T. Nguyen, 2020: Precipitation processes and vertical alignment during the intensification of a weak tropical cyclone in moderate vertical shear. *Mon. Wea. Rev.*, **148**, 1899–1929, https://doi.org/10.1175/MWR-D-19-0315.1.

Sanger, N. T., M. T. Montgomery, R. K. Smith, and M. M. Bell, 2014: An observational study of tropical cyclone spinup in Supertyphoon Jangmi (2008) from 24 to 27 September. *Mon. Wea. Rev.*, **142**, 3–28, https://doi.org/10.1175/MWR-D-12-00306.1.

Sapp, J. W., S. O. Alsweiss, Z. Jelenak, P. S. Chang, and J. Carswell, 2019: Stepped frequency microwave radiometer wind-speed retrieval improvements. *Remote Sens.*, **11**, 214, https://doi.org/10.3390/rs11030214.

Schneider, R., and G. M. Barnes, 2005: Low-level kinematic, thermodynamic, and reflectivity fields associated with Hurricane Bonnie (1998) at landfall. *Mon. Wea. Rev.*, **133**, 3243–3259, https://doi.org/10.1175/MWR3027.1.

Schwendike, J., and J. D. Kepert, 2008: The boundary layer winds in Hurricanes Danielle (1998) and Isabel (2003). *Mon. Wea. Rev.*, **136**, 3168–3192, https://doi.org/10.1175/2007MWR2296.1.

Sears, J., and C. S. Velden, 2012: Validation of satellite-derived atmospheric motion vectors and analyses around tropical disturbances. *J. Appl. Meteor. Climatol.*, **51**, 1823–1834, https://doi.org/10.1175/JAMC-D-12-024.1.

Simpson, R. H., P. K. Govind, and R. Holle, 1975: The GATE dropwindsonde program. *Bull. Amer. Meteor. Soc.*, **56**, 984–987, https://doi.org/10.1175/1520-0477-56.9.984.

Snaiki, R., and T. Wu, 2018: A semi-empirical model for mean wind velocity profile of landfalling hurricane boundary layers. *J. Wind Eng. Ind. Aerodyn.*, **180**, 249–261, https://doi.org/10.1016/j.jweia.2018.08.004.

Stern, D. P., and G. H. Bryan, 2018: Using simulated dropsondes to understand extreme updrafts and wind speeds in tropical cyclones. *Mon. Wea. Rev.*, **146**, 3901–3925, https://doi.org/10.1175/MWR-D-18-0041.1.

——, ——, and S. D. Aberson, 2016: Extreme low-level updrafts and wind speeds measured by dropsondes in tropical cyclones. *Mon. Wea. Rev.*, **144**, 2177–2204, https://doi.org/10.1175/MWR-D-15-0313.1.

——, ——, C. Lee, and J. D. Doyle, 2021: Estimating the risk of extreme wind gusts in tropical cyclones using idealized large-eddy simulations and a statistical–dynamical model. *Mon. Wea. Rev.*, **149**, 4183–4204, https://doi.org/10.1175/MWR-D-21-0059.1.

Torn, R. D., 2014: The impact of targeted dropwindsonde observations on tropical cyclone intensity forecasts of four weak systems during PREDICT. *Mon. Wea. Rev.*, **142**, 2860–2878, https://doi.org/10.1175/MWR-D-13-00284.1.

——, and G. J. Hakim, 2008: Ensemble-based sensitivity analysis. *Mon. Wea. Rev.*, **136**, 663–677, https://doi.org/10.1175/2007MWR2132.1.

Uhlhorn, E. W., and P. G. Black, 2003: Verification of remotely sensed sea surface winds in hurricanes. *J. Atmos. Oceanic Technol.*, **20**, 99–116, https://doi.org/10.1175/1520-0426(2003)020<0099:VORSSS>2.0.CO;2.

——, ——, J. L. Franklin, M. Goodberlet, J. Carswell, and A. S. Goldstein, 2007: Hurricane surface wind measurements from an operational stepped frequency microwave radiometer. *Mon. Wea. Rev.*, **135**, 3070–3085, https://doi.org/10.1175/MWR3454.1.

——, B. W. Klotz, T. Vukicevic, P. D. Reasor, and R. F. Rogers, 2014: Observed hurricane wind speed asymmetries and relationships to motion and environmental shear. *Mon. Wea. Rev.*, **142**, 1290–1311, https://doi.org/10.1175/MWR-D-13-00249.1.

Vickery, P. J., D. Wadhera, M. D. Powell, and Y. Chen, 2009: A hurricane boundary layer and wind field model for use in engineering applications. *J. Appl. Meteor. Climatol.*, **48**, 381–405. https://doi.org/10.1175/2008JAMC1841.1.

Wadler, J. B., J. A. Zhang, B. Jaimes, and L. K. Shay, 2018: Downdrafts and the evolution of boundary layer thermodynamics in Hurricane Earl (2010) before and during rapid intensification. *Mon. Wea. Rev.*, **146**, 3545–3565, https://doi.org/10.1175/MWR-D-18-0090.1.

——, J. J. Cione, J. A. Zhang, E. A. Kalina, and J. Kaplan, 2022: The effects of environmental wind shear direction on tropical cyclone boundary layer thermodynamics and intensity change from multiple observational datasets. *Mon. Wea. Rev.*, **150**, 115–134, https://doi.org/10.1175/MWR-D-21-0022.1.

Wick, G. A., T. F. Hock, P. J. Neiman, H. Vömel, M. L. Black, and J. R. Spackman, 2018: The NCAR-NOAA Global Hawk dropsonde system. *J. Atmos. Oceanic Technol.*, **35**, 1585–1604, https://doi.org/10.1175/JTECH-D-17-0225.1.

Wroe, D. R., and G. M. Barnes, 2003: Inflow layer energetics of Hurricane Bonnie (1998) near landfall. *Mon. Wea. Rev.*, **131**, 1600–1612, https://doi.org/10.1175//2547.1.

Wu, C.-C., J.-H. Chen, P.-H. Lin, and K.-H. Chou, 2007a: Targeted observations of tropical cyclone movement based on the adjoint-derived sensitivity steering vector. *J. Atmos. Sci.*, **64**, 2611–2626, https://doi.org/10.1175/JAS3974.1.

——, K.-H. Chou, P.-H. Lin, S. D. Aberson, M. S. Peng, and T. Nakazawa, 2007b: The impact of dropwindsonde data on typhoon track forecasts in DOTSTAR. *Wea. Forecasting*, **22**, 1157–1176, https://doi.org/10.1175/2007WAF2006062.1.

Wu, T.-C., H. Liu, S. J. Majumdar, C. Velden, and J. L. Anderson, 2014: Influence of assimilating satellite-derived atmospheric motion vector observations on numerical analyses and forecasts of tropical cyclone track and intensity. *Mon. Wea. Rev.*, **142**, 49–71, https://doi.org/10.1175/MWR-D-13-00023.1.

Xie, B., F. Zhang, Q. Zhang, J. Poterjoy, and Y. Weng, 2013: Observing strategy and observation targeting for tropical cyclones using ensemble-based sensitivity analysis and data assimilation. *Mon. Wea. Rev.*, **141**, 1437–1453, https://doi.org/10.1175/MWR-D-12-00188.1.

Yamaguchi, M., T. Iriguchi, T. Nakazawa, and C.-C. Wu, 2009: An observing system experiment for Typhoon Conson (2004) using a singular vector method and DOTSTAR data. *Mon. Wea. Rev.*, **137**, 2801–2816, https://doi.org/10.1175/2009MWR2683.1.

Zawislak, J., and E. J. Zipser, 2010: Observations of seven African easterly waves in the East Atlantic during 2006. *J. Atmos. Sci.*, **67**, 26–43, https://doi.org/10.1175/2009JAS3118.1.

——, and ——, 2014: Analysis of the thermodynamic properties of developing and non developing tropical disturbances using a comprehensive dropsonde dataset. *Mon. Wea. Rev.*, **142**, 1250–1264, https://doi.org/10.1175/MWR-D-13-00253.1.

——, H. Jiang, G. R. Alvey III, E. J. Zipser, R. F. Rogers, J. A. Zhang, and S. N. Stevenson, 2016: Observations of the structure and evolution of Hurricane Edouard (2014) during intensity change. Part I: Relationship between the thermodynamic structure and precipitation. *Mon. Wea. Rev.*, **144**, 3333–3354, https://doi.org/10.1175/MWR-D-16-0018.1.

——, and Coauthors, 2022: Accomplishments of NOAA's Airborne Hurricane Field Program and a broader future approach to forecast improvement. *Bull. Amer. Meteor. Soc.*, **103**, E311–E338, https://doi.org/10.1175/BAMS-D-20-0174.1.

Zhang, J. A., and W. M. Drennan, 2012: An observational study of vertical eddy diffusivity in the hurricane boundary layer. *J. Atmos. Sci.*, **69**, 3223–3236, https://doi.org/10.1175/JAS-D-11-0348.1.

——, and E. W. Uhlhorn, 2012: Hurricane sea surface inflow angle and an observation-based parametric model. *Mon. Wea. Rev.*, **140**, 3587–3605, https://doi.org/10.1175/MWR-D-11-00339.1.
——, W. M. Drennan, P. G. Black, and J. R. French, 2009: Turbulence structure of the hurricane boundary layer between the outer rainbands. *J. Atmos. Sci.*, **66**, 2455–2467, https://doi.org/10.1175/2009JAS2954.1.
——, R. F. Rogers, D. S. Nolan, and F. D. Marks Jr., 2011: On the characteristic height scales of the hurricane boundary layer. *Mon. Wea. Rev.*, **139**, 2523–2535, https://doi.org/10.1175/MWR-D-10-05017.1.
——, ——, P. D. Reasor, E. W. Uhlhorn, and F. D. Marks Jr., 2013: Asymmetric hurricane boundary layer structure from dropsonde composites in relation to the environmental vertical wind shear. *Mon. Wea. Rev.*, **141**, 3968–3984, https://doi.org/10.1175/MWR-D-12-00335.1.
——, D. S. Nolan, R. F. Rogers, and V. Tallapragada, 2015: Evaluating the impact of improvements in the boundary layer parameterization on hurricane intensity and structure forecasts in HWRF. *Mon. Wea. Rev.*, **143**, 3136–3315, https://doi.org/10.1175/MWR-D-14-00339.1.
——, J. J. Cione, E. A. Kalina, E. W. Uhlhorn, T. Hock, and J. A. Smith, 2017: Observations of infrared sea surface temperature and air–sea interaction in Hurricane Edouard (2014) using GPS dropsondes. *J. Atmos. Oceanic Technol.*, **34**, 1333–1349, https://doi.org/10.1175/JTECH-D-16-0211.1.
——, R. Atlas, G. D. Emmitt, L. Bucci, and K. Ryan, 2018: Airborne Doppler wind lidar observations of the tropical cyclone boundary layer. *Remote Sens.*, **10**, 825, https://doi.org/10.3390/rs10060825.
——, E. A. Kalina, M. K. Biswas, R. F. Rogers, P. Zhu, and F. D. Marks, 2020: A review and evaluation of planetary boundary layer parameterizations in Hurricane Weather Research and Forecasting Model using idealized simulations and observations. *Atmosphere*, **11**, 1091, https://doi.org/10.3390/atmos11101091.
Zhang, X., Q. Xiao, and P. J. Fitzpatrick, 2006: The impact of multi satellite data on the initialization and emulation of Hurricane Lili's (2002) rapid weakening phase. *Mon. Wea. Rev.*, **135**, 526–548, https://doi.org/10.1175/MWR3287.1.
Zipser, E. J., and Coauthors, 2009: The Saharan Air layer and the fate of African easterly waves: NASA's AMMA field study of tropical cyclogenesis. *Bull. Amer. Meteor. Soc.*, **90**, 1137–1156, https://doi.org/10.1175/2009BAMS2728.1.